Generation of entropy and forced convection of heat in a conduit partially filled with porous media- Local thermal non-equilibrium and exothermicity effects

Mohsen Torabi [*,a,c], Nader Karimi[b], Kaili Zhang [c], G.P. Peterson [a]

[a] The George W. Woodruff School of Mechanical Engineering, Georgia Institute of Technology, Atlanta, GA 30332, USA

[b] School of Engineering, University of Glasgow, Glasgow G12 8QQ, United Kingdom

[c] Department of Mechanical and Biomedical Engineering, City University of Hong Kong, 83 Tat Chee Avenue, Kowloon, Hong Kong

Abstract

The performance of a two-dimensional, axisymmetric channel with porous inserts attached to the walls is analyzed from the perspective of the first and second laws of thermodynamics. In this analysis, the flow is assumed to be fully developed with a constant heat flux imposed on the external surfaces of the walls, while heat could be internally generated by the fluid and solid phases. Using a Darcy-Brinkman model of momentum transport along with a two-equation thermal energy model, a convective model was developed to describe the thermal boundary conditions on the porous-fluid interface. The so-called Model A was employed on the walls of the channel and semi-analytical solutions were developed for the hydrodynamic, temperature, entropy generation fields and the Nusselt number, and an extensive parametric study was subsequently, conducted. The results indicated that the inclusion of exothermicity leads to significant modifications in the thermal and entropic behaviour of the system. In particular, through comparison with the recent literature, it was demonstrated that exothermicity can significantly impact the influence of the porous-fluid interface model upon the generation of both the local and total entropy within the system.

Keywords: Entropy generation; Local thermal non-equilibrium; Porous media; Exothermicity, Partially-filled conduits.

Nomenclature

a_{sf}	interfacial area per unit volume of porous media, m^{-1}	T_s	temperature of the solid phase of the porous medium, K
Bi	Biot number	T_w	lower wall temperature, K
Bi_{int}	interface Biot number	U_{f1}	dimensionless velocity of the fluid in the clear region
Br	Brinkman number	U_{f2}	dimensionless velocity of the fluid in the porous medium

* Corresponding author
Contact: Mohsen.Torabi@my.cityu.edu.hk, Mohsen.Torabi@me.gatech.edu (M. Torabi), Nader.Karimi@glasgow.ac.uk (N. Karimi).

c_p	specific heat at constant pressure, $\mathrm{J\cdot Kg^{-1}\cdot K^{-1}}$	U_m	dimensionless mean velocity of the fluid
Da	Darcy defined in Eq. (13)	u_{f1}	velocity of the fluid in the porous medium, $\mathrm{m\cdot s^{-1}}$
h	one half of the channel height, m	u_{f2}	velocity of the fluid in the clear region, $\mathrm{m\cdot s^{-1}}$
h_c	one half of the thickness of the clear section, m	u_m	mean velocity of the fluid, $\mathrm{m\cdot s^{-1}}$
h_{sf}	fluid-to-solid heat transfer coefficient, $\mathrm{W\cdot m^{-2}\cdot K^{-1}}$	w_f	dimensionless energy source in fluid phase per unit volume, $\mathrm{W\cdot m^{-3}}$
k	ratio of effective solid thermal conductivity to that of fluid	w_s	dimensionless energy source in solid phase per unit volume, $\mathrm{W\cdot m^{-3}}$
k_{ef}	effective thermal conductivity of the fluid (εk_f), $\mathrm{W\cdot m^{-1}\cdot K^{-1}}$	X	dimensionless axial distance
k_{es}	effective thermal conductivity of the solid $((1-\varepsilon)k_s)$, $\mathrm{W\cdot m^{-1}\cdot K^{-1}}$	x	axial distance, m
N'''_{f1}	dimensionless local entropy generation rate within the clear fluid region	Y	dimensionless vertical distance
N'''_{f2}	dimensionless local entropy generation rate within the fluid phase of the porous medium	Y_c	dimensionless one half of the thickness of the clear section
N'''_s	dimensionless local entropy generation rate within the solid phase of the porous medium	y	vertical distance, m
N_t	dimensionless total entropy generation rate within the medium	**Greek symbols**	
Nu	Nusselt number	ε	porosity
Pe	Peclet number	γ	ratio of the heat flux at porous-fluid interface to that of channel's wall
$\dot{S}'''_{f1}$	local entropy generation rate within the clear fluid region, $\mathrm{W\cdot m^{-3}\cdot K^{-1}}$	κ	permeability, $\mathrm{m^2}$
$\dot{S}'''_{f2}$	local entropy generation rate within the fluid phase of the porous medium, $\mathrm{W\cdot m^{-3}\cdot K^{-1}}$	μ_f	fluid viscosity, $\mathrm{Kg\cdot m^{-1}\cdot s^{-1}}$
$\dot{S}'''_s$	local entropy generation rate within the solid phase of the porous medium, $\mathrm{W\cdot m^{-3}\cdot K^{-1}}$	μ_{eff}	effective viscosity of porous medium, $\mathrm{Kg\cdot m^{-1}\cdot s^{-1}}$
s_f	energy source in fluid phase per unit volume, $\mathrm{W\cdot m^{-3}}$	θ	dimensionless temperature
s_s	energy source in solid phase per unit volume, $\mathrm{W\cdot m^{-3}}$	θ_{f1}	dimensionless temperature of the fluid within clear region
T	temperature, K	θ_{f2}	dimensionless temperature of the fluid phase of the porous medium
T_{f1}	temperature of the fluid within clear region, K	$\theta_{f,m}$	dimensionless mean temperature of the fluid
T_{f2}	temperature of the fluid phase of the porous medium, K	θ_s	dimensionless temperature of the solid phase of the porous medium
$T_{f,m}$	mean temperature of fluid, K	ρ	fluid density, $\mathrm{Kg\cdot m^{-3}}$

1. Introduction

Traditionally, improvement in the performance of thermal systems has focused primarily on the heat transfer aspects [1]. Although this approach is fundamentally sound, it does not account for the degradation of the energy within the system. The key thermodynamic parameter determining the level of energy degradation is the entropy, which can be used to indicate the level of irreversibility within the system [2]. Calculation of the entropy generation rate requires a knowledge of the temperature and flow fields and therefore typically builds upon the heat transfer analysis [3,4]. Entropy generation has been investigated in a number of different types of thermal systems [3–8]. Nevertheless, second law analyses of complex media, such as porous materials are still in the development phase. Currently, there exists a large volume of literature on the heat transfer analysis in porous media [9–11], and a large portion of this work is based on the concept of local thermal equilibrium (LTE). Even though the LTE assumption results in a reasonably good approximation for many applications, there are groups of problems in which LTE may be either inappropriate or inadequate [9,10]. For example, systems with low internal Biot number or those with very different fluid and solid conductivities feature strong non-equilibrium behaviour. Under such circumstances, the more general approach of local thermal non-equilibrium (LTNE) may be preferable. Yet, this approach continues to be challenged by the unresolved issues associated with the definition of the proper thermal boundary conditions at the interface of the porous material [12–14]. Recent studies have indicated that LTNE predictions of the thermal behaviour for a given system is significantly dependent upon these assumed boundary conditions [15–17].

Over the last decade, partially-filled porous conduits have attracted considerable attention mainly due to the hydraulic superiority when compared with fully-filled channels [17-19]. The assumption of LTE has been used extensively to analyze heat transfer processes in the partially-filled systems [11]. Recently, LTNE analyses of these systems have also appeared in the literature. Forooghi et al. [18] conducted a numerical study on a channel, partially filled with a porous insert attached to the walls of the duct. In this investigation, the hydrodynamic field and the Nusselt number were calculated and indicated that the change in Nusselt number with porous thickness is not monotonic [18]. Yang and Vafai [15] considered a channel with a central porous insert and analysed the effects of thermal dispersion and the inertia parameter on the temperature fields and heat transfer enhancement. The results demonstrated that when the condition of temperature gradient equality at the porous interface is not imposed, the heat flux can bifurcate [15]. In a separate work, Yang and Vafai [19] investigated the validity of LTNE in a partially filled conduit under five different interface models to understand the influence of each of these models. Further theoretical investigations were conducted by Xu et al. on a parallel-plate channel [20] and a pipe, partially filled with porous media attached to the inner walls of each geometry [21]. Analytical expressions were developed for the velocity and temperature fields through solution of the hydrodynamic equations in the clear and porous regions and the two-equation energy model [20,21]. Following the work of Ochoa-Tapia and Whitaker [22], Xu et al. [20,21] considered the convective boundary conditions at the porous material-fluid interface. The temperature distributions were calculated under varying thermo-physical parameters and showed that Nusselt number decreases if the channel is fully filled with the porous media [20,21]. Recently, Karimi et al. [23] conducted an analytical study on a channel with a central porous insert, in which both phases included internal heat sources. These authors [23] applied Models

A and B [15,19] to the porous-fluid interface and found the temperature distributions in the solid and fluid phases. In keeping with the earlier findings of Refs. [16,17,24], Karimi et al. demonstrated that the choice of porous-fluid interface model could significantly impact the thermal behaviour of the system [23].

The generation of entropy in porous media has been investigated by a number of individuals. Hooman and Ejlali [25] numerically solved the Darcy-Brinkman model and the one-equation energy model for a fully filled porous pipe under developing conditions. The rate of entropy generation and Bejan number were calculated [25]. In a follow on study, the effects of viscous dissipation on the temperature field and entropy generation in a fully filled channel were investigated by Hooman and Haji Sheikh [26], who conducted an extensive numerical study and showed that under isothermal wall heating, viscous dissipation reduces the Nusselt number in the developing and fully developed regions [26]. In an attempt to provide optimization guides for the fully-filled porous channels, Hooman et al. [27] analytically solved the Darcy-Brinkman model and the LTE energy equation. Three different boundary conditions on the external surface of the channel were considered, and expressions for the Nusselt number, Bejan number and rates of entropy generation were developed. This analysis was later extended to developing flow by considering simple Darcian flow with the LTE condition, under constant temperature boundary conditions [28]. Mahmud and Fraser [29] considered constant, but dissimilar wall temperatures and conducted analytical and numerical studies on the heat transfer and entropy generation characteristics of a fully-filled channel [29]. This investigation was later extended to the case of unsteady flow by Kamish [30]. Further, unsteady heat transfer, fluid flow and entropy generation through a metal foam was investigated analytically by Mahmud et al. [31]. In this study, the governing equations were linearized and analytical expressions were derived for the Nusselt number and entropy generation rate [31]. In a separate work, Mahmud and Fraser [32] calculated the rate of entropy generation during the natural convection of heat in a porous cavity under magneto-hydrodynamic effects.

Entropy generation in unsteady flows in porous media has also been investigated by Tasnim et al. [33] using both theoretical and experimental approaches. In the theoretical investigation, Morosuk [34] demonstrated that the maximum rate of entropy generation in a partially-filled channel occurs at the porous-fluid interface. Entropy generation minimization was used as a design criterion in porous heaters by Shakouhmand et al. [35], who calculated the optimal porosity for a fully-filled porous conduit and showed that the optimum matrix porosity increases with Reynolds number [35]. More recently, Mahdavi et al. [36] conducted a numerical study on partially-filled conduits and calculated the flow field, Nusselt number and entropy generation rates. The results highlighted the effects of porous insert placement and demonstrated that thermal conductivity ratio can dominate the level of heat transfer enhancement [36].

In all of the aforementioned studies the calculation of the entropy generation assumed LTE. Under LTNE, conditions entropy generation is due not only to the viscous dissipation and internal and external heat transfer, these internal heat exchanges introduce an important mechanism of irreversibility. Given this, it is surprising that there are currently only a very limited number of LTNE studies on the entropy generation in porous systems. In a recent work, Buonomo et al. [38] studied porous filled micro channels with LTNE conditions. The hydrodynamic and thermal processes between two parallel plates filled with a porous medium were investigated [38]. This investigation

provided analytical expressions for the velocity and temperature fields, as well as the local and total entropy generation rates [38].

Somewhat later, Torabi et al. [39] considered a horizontal channel partially-filled with porous media under LTNE conditions and analyzed both the heat transfer and the entropy generation. The investigation considered asymmetric boundary conditions for the channel and incorporated the viscous dissipation term into the energy equations [39]. More importantly, these authors reported a bifurcation phenomenon for the local entropy generation rate [39]. Most recently, Torabi et al. [39] conducted heat transfer and entropy generation analyses in a channel partially-filled with porous media using Model A at the porous-fluid interface [40]. This model assumes that the temperatures for both the fluid and solid phases at the porous-fluid interface are equal [40]. The results [39] reported various thermal and thermodynamic characteristics of the system and investigated the effects of the employed porous-fluid interface boundary conditions. Yet, given the significance of the porous-fluid interface model on the thermal behaviour of partially-filled systems [23], the sensitivity of the results [39] on the changes in the porous-fluid interface model was not clear.

The review of the literature reveals the following:

- The porous-fluid thermal interface model is an essential factor in the determination of the thermal characteristics of the partially-filled system. However, there is currently no generally applicable thermal porous-fluid interface model [16,17,23]. As a result, a given system is often analyzed with different interface models in order to develop a more complete picture of the system behavior [16,17,23,24].
- Minimization of the entropy generation presents a methodology by which the thermal system can be optimized. The accuracy of this method is directly dependent upon the precise evaluation of all of the irreversibilities present within the system.
- Non-equilibrium internal heat transfer is an important irreversibility in porous media. However, so far, the problem of entropy generation under LTNE has received little attention.

These results clearly, indicate the need for further studies on the fundamentals of LTNE heat transfer and the second law analysis of partially-filled systems. The current work is focused on addressing this issue through an analytical study. Figure 1 illustrates a schematic view of the problem under investigation. Fluid moves into a channel, in which porous inserts are attached to the inner walls. A constant heat-flux boundary condition is imposed on the walls of the channel. The height of the channel is $2h$ and the core, with the thickness $2h_c$, is clear. Due to the symmetry of the configuration only half of the channel is considered.

2. Theoretical methods

2.1. Governing equations and assumptions

The proceeding analyses are on the basis of the following assumptions. The porous medium is homogenous, isotropic and fluid saturated and, the flow is steady, laminar and incompressible. Thermally and hydrodynamically

fully developed conditions hold in both clear and porous regions of the channel. Natural convection, radiative heat transfer and thermal dispersion effects are ignored. Physical properties of the solid matrix and the fluid such as porosity, specific heat, density and thermal conductivity are invariants. Further, heat is generated or consumed uniformly and steadily throughout the fluid and solid phases. However, viscous dissipation is neglected in energy equations, both for the clear and porous sections. It should be noted that the constant heat sources in the solid and fluid phases of the porous media may represent various physical and chemical processes. These include, dissipation of electrical energy, absorption or radiation of infrared, gamma and beta waves and also nuclear and chemical reactions [23,40–45].

Given these assumptions, the governing equations for the transport of momentum and heat are simplified to the followings. Momentum equations in the clear and porous regions can be, respectively, written as

$$-\frac{\partial p}{\partial x}+\mu_f \frac{\partial^2 u_{f1}}{\partial y^2}=0 \qquad 0\le y\le h_c\,, \tag{1a}$$

$$-\frac{\partial p}{\partial x}+\mu_{eff} \frac{\partial^2 u_{f2}}{\partial y^2}-\frac{\mu_f}{\kappa}u_{f2}=0 \quad h_c\le y<h\,. \tag{1b}$$

Equation (1b) is the Darcy-Brinkman model of momentum transport in porous media [11]. Considering LTNE the transport of thermal energy in the fluid and solid phases are written as

$$\rho c_p u_{f1}\frac{\partial T_{f1}}{\partial x}=k_f \frac{\partial^2 T_{f1}}{\partial y^2}+s_f \qquad 0\le y\le h_c\,, \tag{2a}$$

$$\rho c_p u_{f2}\frac{\partial T_{f2}}{\partial x}=k_{ef} \frac{\partial^2 T_{f2}}{\partial y^2}+h_{sf}\,a_{sf}\left(T_s-T_{f2}\right)+s_f \quad h_c\le y<h\,, \tag{2b}$$

$$0=k_{es}\frac{\partial^2 T_s}{\partial y^2}-h_{sf}\,a_{sf}\left(T_s-T_{f2}\right)+s_s \quad h_c\le y<h\,, \tag{2c}$$

The boundary conditions for the momentum and energy equations are given by,

$$y=0: \frac{\partial u_{f1}}{\partial y}=0,\ \frac{\partial T_{f1}}{\partial y}=0\,, \tag{3a}$$

$$\begin{aligned} &y=h_c: u_{f1}=u_{f2},\ \mu_f\frac{\partial u_{f1}}{\partial y}=\mu_{eff}\frac{\partial u_{f2}}{\partial y},\ q_{\text{int}}=k_f\frac{\partial T_{f1}}{\partial y}=k_{ef}\frac{\partial T_{f2}}{\partial y}+k_{es}\frac{\partial T_s}{\partial y},\\ &T_{f1}=T_{f2},\ k_{es}\frac{\partial T_s}{\partial y}=h_{sf}\left(T_s-T_{f1}\right) \end{aligned}\,, \tag{3b}$$

$$y = h : u_{f2} = 0, T_{f2} = T_s = T_w, q_w = k_{ef} \frac{\partial T_{f2}}{\partial y} + k_{es} \frac{\partial T_s}{\partial y} . \quad (3c)$$

The boundary conditions expressed by Eqs. (3b) set a convective thermal model of porous-fluid interface and were used previously by Xu et al. [20,21]. It is essential to note that these boundary conditions are different to those of Refs. [16,17,24], which are on the basis of the phenomenological interface models of Yang and Vafai [15]. Here, Model A of Yang and Vafai [15] is used to specify the thermal boundary condition on the solid-porous interface at the inner walls of the channel. Equation (3b) is amongst the central parts of the current analysis and differentiates it from the previous analyses [39].

In order to convert the set of partial differential equations (2a) and (2b) to ordinary differential equations, i.e, obtaining a constant value for differentiation of fluid's temperature versus horizontal direction, a special mathematical manipulation is needed. By an integration over Eq. (2a), and taking into account the boundary conditions at the centreline of the channel and the interface of the clear section and the porous medium, the following formulation is achieved:

$$\rho c_p \frac{\partial T_{f1}}{\partial x} \int_0^{h_c} u_{f1} \mathrm{d}y = \underbrace{k_f \int_0^{h_c} \frac{\partial^2 T_{f1}}{\partial y^2} \mathrm{d}y}_{q_{\mathrm{int}}} + \int_0^{h_c} s_f \, \mathrm{d}y . \quad (4)$$

This procedure is repeated to achieve the derivation of fluid's temperature versus horizontal direction in Eq. (2b), by adding Eqs. (2b) and (2c) and integrating from the interface and the upper wall of the channel, the following is given:

$$\rho c_p \frac{\partial T_{f2}}{\partial x} \int_{h_c}^{h} u_{f2} \mathrm{d}y = \underbrace{k_{ef} \int_{h_c}^{h} \frac{\partial^2 T_{f2}}{\partial y^2} \mathrm{d}y + k_{es} \int_{h_c}^{h} \frac{\partial^2 T_s}{\partial y^2} \mathrm{d}y}_{q_w - q_{\mathrm{int}}} + \int_{h_c}^{h} \left(s_f + s_s \right) \mathrm{d}y . \quad (5)$$

Noting that in fully developed flow under constant wall heat flux $\frac{\partial T_{f2}}{\partial x} = \frac{\partial T_{f1}}{\partial x} = \text{constant}$, and taking into account both Eqs. (4) and (5), the left hand side of Eqs. (2a) and (2b) turns to

$$\rho c_p \frac{\partial T_{f1}}{\partial x} = \rho c_p \frac{\partial T_{f2}}{\partial x} = \frac{q_w + \int_0^h s_f \, \mathrm{d}y + \int_{h_c}^h s_s \mathrm{d}y}{h u_m} , \quad (6)$$

in which,

$$u_m = \frac{1}{h} \left(\int_0^{h_c} u_{f1} \mathrm{d}y + \int_{h_c}^{h} u_{f2} \mathrm{d}y \right) . \quad (7)$$

Substituting Eq. (6) into Eqs. (2a) and (2b), results in the following energy equations for the fluid flow in the clear and porous regions,

$$u_{f1}\frac{q_w+\int_0^h s_f\,\mathrm{d}y+\int_{h_c}^h s_s\,\mathrm{d}y}{hu_m}=k_f\,\frac{\partial^2 T_{f1}}{\partial y^2}+s_f \qquad 0\le y\le h_c\,, \tag{8a}$$

$$u_{f2}\frac{q_w+\int_0^h s_f\,\mathrm{d}y+\int_{h_c}^h s_s\,\mathrm{d}y}{hu_m}=k_{ef}\,\frac{\partial^2 T_{f2}}{\partial y^2}+h_{sf}\,a_{sf}\,\left(T_s-T_{f2}\right)+s_f \qquad h_c\le y<h\,. \tag{8b}$$

The Nusselt number at the wall of the channel is, often, written as [20,21,46,47]

$$Nu=\frac{4h\times q_w}{k_f\left(T_{f1,w}-T_{f,m}\right)}\,. \tag{9}$$

where

$$T_{f,m}=\frac{1}{hu_m}\left(\int_0^{h_c}u_{f1}T_{f1}\mathrm{d}y+\int_{h_c}^h u_{f2}T_{f2}\mathrm{d}y\right). \tag{10}$$

Under LTE conditions, Eqs. (2b) and (2c) can be combined to form a single energy equation for the porous region. The energy equation for the clear fluid flow and the LTE energy equation for the porous region can be written as

$$\rho c_p u_{f1}\frac{\partial T_{f1}}{\partial x}=k_f\,\frac{\partial^2 T_{f1}}{\partial y^2}+s_f \qquad 0\le y\le h_c\,, \tag{11a}$$

$$\rho c_p u_{f2}\frac{\partial T_{f2}}{\partial x}=\left(k_{ef}+k_{es}\right)\frac{\partial^2 T_{f2}}{\partial y^2}+s_f+s_s \qquad h_c\le y<h\,. \tag{11b}$$

LTE assumption in Eq. (11b) requires equality of temperatures in solid and fluid phases inside the porous medium $T_{f2}=T_s$. Hence, the LTE thermal boundary conditions reduce to the followings.

$$y=0:\frac{\partial T_{f1}}{\partial y}=0\,, \tag{12a}$$

$$y=h_c:q_{\mathrm{int}}=k_f\,\frac{\partial T_{f1}}{\partial y}=\left(k_{ef}+k_{es}\right)\frac{\partial T_{f2}}{\partial y},\,T_{f1}=T_{f2}\,, \tag{12b}$$

$$y=h:T_{f2}=T_w\,,\,q_w=\left(k_{ef}+k_{es}\right)\frac{\partial T_{f2}}{\partial y}\,. \tag{12c}$$

2.2. Normalisation

The pertinent parameters can be combined to form a number of dimensionless groups:

$$U=\frac{u}{u_r},\ \theta=\frac{k_{es}\left(T-T_w\right)}{q_w h},\ k=\frac{k_{es}}{k_{ef}}=\frac{\left(1-\varepsilon\right)k_s}{\varepsilon k_f},\ Bi=\frac{h_{sf}a_{sf}h^2}{k_{es}},\ Bi_{\text{int}}=\frac{h_{sf}h}{k_{es}},\ Y=\frac{y}{h},\ X=\frac{x}{h},$$
$$Y_c=\frac{h_c}{h},\ Da=\frac{\kappa}{h^2},\ Br=\frac{\mu_f u_r^2}{q_w h},\ Pe=\frac{\rho c_p u_r h}{k_{ef}},\ \gamma=\frac{q_{\text{int}}}{q_w},\ w_f=\frac{s_f h}{q_w},\ w_s=\frac{s_s h}{q_w},\ B=\frac{k_{ef}T_w}{q_w h} \tag{13}$$

where $u_r=-\frac{h^2}{\mu_f}\frac{\partial p}{\partial x}$. The dimensionless groups are then substituted into the momentum Eqs. (1a) and (1b), energy Eqs. (2c), (8a) and (8b), and boundary Eqs. (3). Momentum Eqs. (1a) and (1b) are now expressed by

$$1+\frac{\partial^2 U_{f1}}{\partial Y^2}=0 \qquad 0\le Y\le Y_c, \tag{14a}$$

$$1+\frac{1}{\varepsilon}\frac{\partial^2 U_{f2}}{\partial Y^2}-\frac{U_{f2}}{Da}=0 \qquad Y_c<Y\le 1. \tag{14b}$$

The dimensionless form of energy Eqs. (2a, b and c) are

$$\frac{AU_{f1}}{U_m}=\frac{1}{\varepsilon k}\frac{\partial^2\theta_{f1}}{\partial Y^2}+w_f \qquad 0\le Y\le Y_c, \tag{15a}$$

$$\frac{AU_{f2}}{U_m}=\frac{1}{k}\frac{\partial^2\theta_{f2}}{\partial Y^2}+Bi\left(\theta_s-\theta_{f2}\right)+w_f \qquad Y_c\le Y\le 1, \tag{15b}$$

$$0=\frac{\partial^2\theta_s}{\partial Y^2}-Bi\left(\theta_s-\theta_{f2}\right)+w_s \qquad Y_c\le Y\le 1. \tag{15c}$$

Further, the hydrodynamic and thermal boundary conditions can be reduced to the following,

$$Y=0:\frac{\partial U_{f1}}{\partial Y}=0,\ \frac{\partial\theta_{f1}}{\partial Y}=0, \tag{16a}$$

$$Y=Y_c:U_{f1}=U_{f2},\ \frac{\partial U_{f1}}{\partial Y}=\frac{1}{\varepsilon}\frac{\partial U_{f2}}{\partial Y},\ \gamma=\frac{1}{\varepsilon k}\frac{\partial\theta_{f1}}{\partial Y}=\frac{1}{k}\frac{\partial\theta_{f2}}{\partial Y}+\frac{\partial\theta_s}{\partial Y},\ \theta_{f1}=\theta_{f2},\ \frac{\partial\theta_s}{\partial Y}=Bi_{\text{int}}\left(\theta_s-\theta_{f1}\right), \tag{16b}$$

$$Y=1:U_{f2}=0,\ 1=\frac{1}{k}\frac{\partial\theta_{f2}}{\partial Y}+\frac{\partial\theta_s}{\partial Y},\ \theta_{f2}=\theta_s=0, \tag{16c}$$

where

$$A = 1 + \int_0^1 w_f \, \mathrm{d}Y + \int_{Y_c}^1 w_s \, \mathrm{d}Y \ , \tag{17a}$$

$$U_m = \int_0^{Y_c} U_{f1} \mathrm{d}Y + \int_{Y_c}^1 U_{f2} \mathrm{d}Y \ . \tag{17b}$$

To decouple Eqs. (15b) and (15c), these are first differentiated twice. After some algebraic manipulation, the decoupled form of the energy equations can be written as

$$\frac{A}{U_m}\frac{\partial^2 U_{f2}}{\partial Y^2} = \frac{1}{k}\frac{\partial^4 \theta_{f2}}{\partial Y^4} + Bi\left(\frac{AU_{f2}}{U_m} - \left(1+\frac{1}{k}\right)\frac{\partial^2 \theta_{f2}}{\partial Y^2} - w_f - w_s\right) + \frac{\partial^2 w_f}{\partial Y^2} \ , \tag{18a}$$

$$0 = \frac{\partial^4 \theta_s}{\partial Y^4} - Bi\left(-\frac{kAU_{f2}}{U_m} + (1+k)\frac{\partial^2 \theta_s}{\partial Y^2} + kw_f + kw_s\right) + \frac{\partial^2 w_s}{\partial Y^2} \, . \tag{18b}$$

Using Eqs. (15b) and (15c) and the respective first derivatives, the following boundary conditions can be derived.

$$Y = 1: \begin{cases} \dfrac{\partial^2 \theta_s}{\partial Y^2} + w_s = 0 \\ \dfrac{1}{k}\dfrac{\partial^2 \theta_{f2}}{\partial Y^2} + w_f = 0 \\ \dfrac{A}{U_m}\dfrac{\partial U_{f2}}{\partial Y} = \dfrac{1}{k}\dfrac{\partial^3 \theta_{f2}}{\partial Y^3} + Bi\left(\dfrac{\partial \theta_s}{\partial Y} - \dfrac{\partial \theta_{f2}}{\partial Y}\right) + \dfrac{\partial w_f}{\partial Y} \\ \dfrac{\partial^3 \theta_s}{\partial Y^3} - Bi\left(\dfrac{\partial \theta_s}{\partial Y} - \dfrac{\partial \theta_{f2}}{\partial Y}\right) + \dfrac{\partial w_s}{\partial Y} = 0 \end{cases} \tag{19}$$

Based upon the dimensionless parameters, the Nusselt number can be expressed as

$$Nu = -\frac{4\varepsilon k}{\theta_{f,m}} \, , \tag{20}$$

where

$$\theta_{f,m} = \frac{1}{U_m}\left(\int_0^{Y_c} U_{f1}\theta_{f1} \mathrm{d}Y + \int_{Y_c}^1 U_{f2}\theta_{f2} \mathrm{d}Y\right). \tag{21}$$

Assuming the LTE condition and using the dimensionless parameters given by Eq. (13), the dimensionless one-equation energy model can be expressed as,

$$\frac{AU_{f1}}{U_m} = \frac{1}{\varepsilon k}\frac{\partial^2 \theta_{f1}}{\partial Y^2} + w_f \qquad 0 \le Y \le Y_c \, , \tag{22a}$$

$$\frac{AU_{f2}}{U_m}=\left(\frac{1}{k}+1\right)\frac{\partial^2\theta_{f2}}{\partial Y^2}+w_f+w_s \qquad Y_c\le Y\le 1. \tag{22b}$$

The thermal boundary conditions for the LTE model are slightly different than those developed earlier for the LTNE model. The boundary conditions for this case can be expressed as follows.

$$Y=0:\frac{\partial\theta_{f1}}{\partial Y}=0, \tag{23a}$$

$$Y=Y_c:\gamma=\frac{1}{\varepsilon k}\frac{\partial\theta_{f1}}{\partial Y}=\left(\frac{1}{k}+1\right)\frac{\partial\theta_{f2}}{\partial Y},\ \theta_{f1}=\theta_{f2}, \tag{23b}$$

$$Y=1:1=\left(\frac{1}{k}+1\right)\frac{\partial\theta_{f2}}{\partial Y},\ \theta_{f2}=0. \tag{23c}$$

2.3. Entropy generation

In the current investigation, the heat transfer over a finite temperature difference and viscous dissipation of the flow kinetic energy both contribute to the irreversibility of the system. The detailed derivations of these equations are given in Refs. [38,42,48].

$$N_{f1}'''=\frac{\dot{S}_{f1}'''h^2}{k_{es}}=\frac{\left[\left(\frac{1+\int_0^1 w_f\,dY+\int_0^{Y_c}w_s\,dY}{(Pe/k)U_m}\right)^2+\left(\frac{\partial\theta_{f1}}{\partial Y}\right)^2\right]}{\varepsilon k\left(\theta_{f1}+B\right)^2}+\frac{Br\left(\frac{\partial U_{f1}}{\partial Y}\right)^2}{\left(\theta_{f1}+B\right)} \quad 0\le Y\le Y_c, \tag{24a}$$

$$N_{f2}'''=\frac{\dot{S}_{f2}'''h^2}{k_{es}}=\frac{\left[\left(\frac{1+\int_0^1 w_f\,dY+\int_0^{Y_c}w_s\,dY}{(Pe/k)U_m}\right)^2+\left(\frac{\partial\theta_{f2}}{\partial Y}\right)^2\right]}{k\left(\theta_{f2}+B\right)^2}+\frac{Bi\left(\theta_s-\theta_{f2}\right)^2}{\left(\theta_s+B\right)\left(\theta_{f2}+B\right)}+\frac{BrU_{f2}^2}{Da\left(\theta_{f2}+B\right)} \tag{24b}$$

$$+\frac{Br\left(\frac{\partial U_{f2}}{\partial Y}\right)^2}{\varepsilon\left(\theta_{f2}+B\right)} \quad Y_c\le Y<1,$$

$$N_s'''=\frac{\dot{S}_s'''h^2}{k_{es}}=\frac{\left[\left(\frac{1+\int_0^1 w_f\,dY+\int_0^{Y_c}w_s\,dY}{(Pe/k)U_m}\right)^2+\left(\frac{\partial\theta_s}{\partial Y}\right)^2\right]}{\left(\theta_s+B\right)^2}+\frac{Bi\left(\theta_s-\theta_{f2}\right)^2}{\left(\theta_s+B\right)\left(\theta_{f2}+B\right)} \quad Y_c\le Y<1, \tag{24c}$$

where the parameter $B = \frac{T_w k_{es}}{q_w h}$. It is worth mentioning that, assuming a reference temperature for the denominators of Eqs. (24a, b and c) considerably decreases the mathematical complexity of the problem. This approach has been utilized in previous investigations [49]. Nevertheless, to enhance the accuracy of the predicted local and total entropy generation rates, the local temperature was used in these equations [50,51]. The dimensionless total entropy generation rate for the channel can be obtained by integrating the dimensionless form of the relations expressing the volumetric local entropy generation, over the height of the channel, which yields

$$N_t = \int_0^{Y_c} N'''_{f1} \mathrm{d}Y + \int_{Y_c}^{1} \left(N'''_{f2} + N'''_{s} \right) \mathrm{d}Y \quad . \tag{25}$$

2.4. Velocity and temperature fields

The momentum and energy equations derived earlier in this section can now be solved analytically revealing the velocity and temperature fields in the porous and clear regions. The solutions for Eqs. (14a) and (14b) yields the velocity field [39].

Solution of the differential energy equations, Eqs. (18a) and (18b), provide the general solution for the temperature distributions within the porous regions. Further, solving Eq. (15a) renders the temperature field in the clear region. These temperature fields can be described as

$$\theta_{f1}=\frac{1}{2}\frac{k\varepsilon\left(-\frac{1}{12}AY^{4}+\frac{1}{3}AC_{1}Y^{3}+AC_{2}Y^{2}-U_{m}w_{f}Y^{2}\right)}{U_{m}}+D_{1}Y+D_{2}, \tag{26a}$$

$$\theta_{f2}=\frac{-1}{\left(A_{1}kDa+\varepsilon\right)}\left(\frac{A_{2}kDa^{2}}{\varepsilon}\cosh\left(\frac{Y}{\sqrt{Da/\varepsilon}}\right)+\frac{A_{3}kDa^{2}}{\varepsilon}\sinh\left(\frac{Y}{\sqrt{Da/\varepsilon}}\right)\right)+\frac{D_{3}\cosh\left(\sqrt{-kA_{1}}Y\right)}{kA_{1}}+\frac{D_{4}\sinh\left(\sqrt{-kA_{1}}Y\right)}{kA_{1}}-\frac{A_{4}}{2A_{1}}Y^{2}+D_{5}Y+D_{6}, \tag{26b}$$

$$\theta_{s}=\frac{-Da^{2}}{\varepsilon\left(B_{1}Da+\varepsilon\right)}\left(B_{2}\cosh\left(\frac{Y}{\sqrt{Da/\varepsilon}}\right)+B_{3}\sinh\left(\frac{Y}{\sqrt{Da/\varepsilon}}\right)\right)-\frac{D_{7}}{B_{1}}\cosh\left(\sqrt{-A_{1}}Y\right)+\frac{D_{8}}{B_{1}}\sinh\left(\sqrt{-A_{1}}Y\right)-\frac{B_{4}}{2B_{1}}Y^{2}+D_{9}Y+D_{10}, \tag{26c}$$

where

$$A_{1}=-Bi-Bi/k,\ A_{2}=\frac{BiAC_{4}}{U_{m}}-\frac{A\varepsilon C_{4}}{DaU_{m}},\ A_{3}=\frac{BiAC_{3}}{U_{m}}-\frac{A\varepsilon C_{3}}{DaU_{m}},\ A_{4}=\frac{BiADa}{U_{m}}-Bi\left(w_{f}+w_{s}\right), \tag{27a}$$

$$B_{1}=-Bi-Bi/k,\ B_{2}=\frac{BikAC_{4}}{U_{m}},\ B_{3}=\frac{BikAC_{3}}{U_{m}},\ B_{4}=\frac{BikADa}{U_{m}}-Bik\left(w_{f}+w_{s}\right). \tag{27b}$$

where the parameters $D_1 - D_{10}$ are calculated numerically using mathematical software, i.e. Maple. The accuracy of the solution procedure has been demonstrated in previous investigations [38,50]. Solution of the LTE energy equation is straightforward and is, therefore, not presented here.

3. Results and discussion

An extensive parametric study was conducted, with particular attention given to the exploration of the effects of internal heat generation on the temperature fields, Nusselt number and entropy generation. To this end, three different combinations of solid and fluid thermal source terms were considered. These include first: $\omega_f = 10, \omega_s = 10$, second: $\omega_f = 10, \omega_s = 0$ and third: $\omega_f = 0, \omega_s = 10$. The equality of the solid and fluid thermal source terms, in case 1, sets a reference case in which heat is uniformly generated within the porous medium. The other two cases are representative of practical engineering problems in which heat is generated in the fluid or solid. Examples for the former can be readily found in chemical reactors while electronics cooling and nuclear reactors are the classical examples of the latter [23,40–45]. It should be noted that in the figures the solid lines refer to the properties of the solid phase and the dashed lines correspond to the fluid phase. For validation of the resulting analytical expressions, it should be note that although not shown here, in the limit of large Biot number the LTNE results approach those of LTE. This is to be expected physically and therefore further supports the validity of the solution procedure. Second, Appendix A shows that in the limit of fully filled channel the LTE solutions of section 2.4 coincide with those of Ref. [45].

3.1. Heat transfer

Figure 2 illustrates the temperature distributions in the solid and fluid phases for a given set of parameters and different values of the thermal conductivity ratio and internal heat generation. Figures 2a and 2b demonstrate that there exists two different routes for swapping the relative hot and cold phases in the porous region. First, variations in the thermal conductivity ratio may lead to the swap of the hot and cold phases. This is illustrated in Fig. 2a which for a low value of the thermal conductivity ratio, the solid phase has the higher dimensionless temperature. However, increasing the value of the thermal conductivity ratio changes this and the fluid phase becomes relatively hotter. The second route for changing the relative hot and cold phases, is at constant thermal conductivity ratio. In Fig. 2a and for the lowest values of *k*, the solid temperature is always greater than that of the fluid. However, by modifying the internal heat generation in Fig. 2b this trend is reversed in the majority of the porous insert. This behaviour is a direct consequence of the convective thermal boundary condition and was not observed under other types of porous-fluid interface models [23]. As a result of swapping the hot and cold phases, the direction of internal heat exchange in the porous medium changes. This is regarded as a bifurcation phenomenon and has been previously observed in other configurations [38]. Figure 2 also shows that occurrence of bifurcation is strongly affected by the internal heat sources. As a result, for the case of an exothermic solid phase and no heat generation in the fluid phase (Fig. 2c) the bifurcation does not occur.

Figures 3a-c illustrate the influence of the thermal boundary conditions at the porous-fluid interfaces upon the temperature fields. In these figures, the Biot number (*Bi)* at the interface varies by two orders of magnitude, while the *Bi* inside the porous insert remains constant. Different combinations of fluid and solid internal heat sources are considered in Figs. 3a-c. These figures clearly indicate that, in general, increasing the interface *Bi* results in an increase in the dimensionless temperatures of the fluid phase. Inversely, increasing the interface *Bi* decreases the dimensionless solid temperature. Alternatively, for the cases shown in Figs. 3a-c the temperature difference between the two phases becomes more appreciable as the value of the interface *Bi* decreases. Further, the internal heat sources appear to have a strong effect upon the behavior of the temperature fields. In Figs. 3a and b the occurrence of bifurcation in the temperature fields is evident, while when the heat source is applied to the solid phase only, there is no bifurcation (Fig. 3c).

Figure 4 illustrates the fluid and solid temperature profiles under varying Biot number and internal heat generation. It is important to note that this *Bi* is different from the interface *Bi* , as the heat convection on the interface is distinctive to that inside the porous material. Interestingly, in Fig. 4 for a *Bi* of order 0.1 and 1 the temperature fields remain almost the same. This is the case for all considered combinations of internal heat sources in Figs. 4a-c. However, further increasing of the *Bi* to 10 causes a considerable drop in the dimensionless temperature and signifies the temperature difference between the wall and the porous medium. It is further noted that in Fig. 4a, and under similar strengths of the internal heat sources the differences between the dimensionless fluid and solid temperatures is independent of the *Bi*. Nonetheless, introduction of the exothermic fluid and solid phase in Figs. 4b and c signifies the temperature difference within the porous medium. This is particularly the case at low and intermediate values of *Bi*. This behaviour appears to be a peculiarity of the exothermic systems and is not usually observed in the systems without internal heat sources [20,21].

Figure 5 illustrates the effects of thickness of the clear section on the temperature fields. Generally, lowering the thicknesses of the clear section results in higher dimensionless temperatures. However, the extent of temperature variations and the differences between the solid and fluid temperatures are largely dependent upon the internal heat sources. Figure 5a shows the variation of the dimensionless temperatures with changes in the thickness of the clear section. These variations appear to be of a lesser extent in Figs. 5b and 5c. Figure 5b shows that for the exothermic fluid, the temperature difference between the solid and fluid is dependent upon the channel configuration. This is such that by widening the gap between the two porous inserts, the solid and fluid dimensionless temperature difference declines. It is also important to note that in keeping with the earlier observations, the case with an exothermic solid (Fig. 5c) does not result in a temperature bifurcation for any value of porous thickness. In Figs. 6a-c values of the internal heat sources have been varied and the resultant temperature fields were calculated. These figures include the case with no internal heat generation as well as two different levels of exothermicity. They confirm that under the selected parameters and for no internal heat source, the solid and fluid temperatures are relatively close to each other and LTE is an acceptable approximation. However, introduction of exothermicity causes noticeable differences between the solid and fluid dimensionless temperatures.

Figures 2-6 demonstrated that, for a given set of parameters, the centre of the channel usually features the largest temperature difference with the wall of the channel. Figure 7 shows the influence of different parameters upon the ~~center~~centre line temperature. As sown in Fig. 7a, upon increasing the thickness of the clear region, the ~~center~~centre line dimensionless temperature first decreases and then reaches a minimum. Further increases in the thickness of the clear region results in a monotonic increase of this temperature. Figure 7b shows that for relatively low and intermediate values of the Darcy number variation of the ~~center~~centre line temperature with the thickness of the clear section, results in an initial drop. This is then followed by a minimum point and a subsequent rise. This pattern changes at higher values of the Darcy number and is replaced by a monotonic increase in the dimensionless temperature. Figure 7c, however, indicates that porosity has a more uniform effect and the ~~center~~centre line temperature always features the same qualitative trend for all values of porosity.

Figure 8 depicts the effects of the thermal conductivity ratio on the LTE and LTNE predictions of the Nusselt number. Here, it is apparent that, in general, the LTE solution tends to overestimate the Nusselt number. This is particularly true for the case of lower values of the thickness of the clear section. As expected, increasing the clear section thickness results in the behaviour of the channel becoming increasingly similar to that of a clear channel. As a result, increasing the thickness of the clear section results in the LTE and LTNE Nusselt numbers approaching each other. Further, the LTE Nusselt number appears to increase with increasing the thermal conductivity ratio. However, this is not generally the case for the LTNE prediction of *Nu*. Depending upon the value of Y_c, the LTNE Nusselt number may either correlate directly or inversely with the thermal conductivity ratio. Consequently, a comparison between the *Nu* with provided interface condition in the present investigation and the previously published article [39] has been given in Fig. 9. It is clearly seen that the interface boundary condition has influential impact on the *Nu* value of the walls' channel, which is from different values of the temperature across the channel compared to the previous interface model [39]. The influence of the Darcy number on the *Nu* are illustrated in Fig. 10. As shown, higher Darcy numbers generally result in higher Nusselt numbers. Nevertheless, there are important exceptions. For instance, while for low values of Y_c the Nusselt numbers at $Da = 10^{-4}$, are smaller than those calculated at $Da = 10^{-3}$ this trend is reversed at $Y_c \cong 0.5$. Figure 10b provides information on the behaviour of *Nu* versus the thickness of the clear section. Starting from a small clear gap and increasing the thickness of the clear section results in a drop in the *Nu* to a minimum. Further increases in the clear section the Nusselt number results in increases for all values of the thermal conductivity ratio. The rate of this increase is dependent on *k* and generally increases with increasing values of *k*. It should also be noted that for low values of Y_c the Nusselt number corresponding to the lowest value of the thermal conductivity ratio, takes a considerably larger value. Finally, it is clear from Fig. 10c that increasing the porosity yields higher Nusselt numbers.

3.2. Local and total generation of entropy

Recently, it has been shown that the arrangement of partially-filled channels can significantly affect the local entropy generation [38]. To better understand this phenomenon, Figs. 11a-c show the changes of the dimensionless local generation of the entropy across the channel for varying thicknesses of the clear region and specify the entropy

generation rates. As shown in Fig. 11a, for the case of equal exothermicity in the fluid and solid phases, the entropy generation in the clear fluid greatly exceeds that in the solid and fluid phases in the porous medium. This figure also indicates that a slight increase in the thickness of the clear section results in a major reduction in the entropy generation. The difference between the entropy generation in the clear and porous regions diminishes and results in a more uniform rate of entropy generation across the channel. This can be attributed to the smaller fluid velocity gradients in the channel with larger clear sections, which leads to less significant viscous dissipation and entropy generation. Limiting the exothermicity to one of the two phases illustrated in Figs. 11b and 11c, while keeping all other parameters constant, results in a substantial decrease in the entropy generation. This is particularly true for the case in shown in Fig. 11c, in which the heat generation is exclusive to the solid phase. The strong dependency of irreversibility on the internal heat generation serves to emphasize the importance of this parameter on the second law analysis of porous systems.

Figure 12 represents the impact of the thermal conductivity ratio on the local entropy generation. Two different values of the thermal conductivity ratio for the fixed channel configuration and three combinations of the internal heat sources were considered. As shown, decreasing the thermal conductivity ratio reduces the value of the rate of the local entropy generation, and as shown in Figs. 12a-c this is consistent with earlier observations of the effect of thermal conductivity ratio on the temperature distributions (Fig. 2). Decreasing the thermal conductivity ratio decreases the temperature differences within the system, which in turn reduces the internal heat exchange between the different components. Consequently, the local entropy generation rate is reduced. Figure 13 illustrates the calculated entropy generation profiles for the two different values of the Darcy number. As expected, a lower Darcy number results in a higher level of entropy generation in both the fluid and solid phases. This is due in part, to the fact that the lower permeability associated with a smaller Darcy number, intensifies the viscous dissipation rate. It also modifies the temperature fields and Nusselt number, which can further increase the rate of entropy generation. Similar to the observations made in Fig. 12, the entropy generation in Fig. 13, is heavily dependent upon the internal heat sources in the channel.

Figures 14a-c illustrate the influence of the thermal conductivity ratio, the Peclet number and the internal heat generation on the total entropy generation of the system. These figures clearly illustrate the substantial effect of the channel configuration, on the total entropy generation within the system. This influence is so strong that increasing the gap between the two porous inserts, can decrease the total entropy generation by several orders of magnitude. Interestingly, variations in the total entropy generation for a given thickness of the clear section, is very strong for $Y_c < 0.5$. However, for values of the thickness of the clear section that are higher than this limit, there is essentially no correlation between the thickness and the total entropy generation. This is an important observation, which clearly reflects the advantage of only partially filling the channel, in comparison with fully-filled porous conduits. Figure 14a shows that k=1 results in the minimization of the total entropy generation. It further indicates that for narrow gaps between the two porous inserts, the rise of thermal conductivity ratio greatly increases the total entropy generation. Similarly, in Fig. 14b, decreasing the Peclet number can significantly intensity the total generation of entropy. Finally, Fig. 14c shows that by increasing the exothermicity in the fluid and solid phases, the total entropy

generation increases rapidly. This is such that for a nearly filled channel, a relatively small increase in the exothermicity can double the total entropy generation. Figure 15 provides an insight into~~on~~ the effect of the *Bi* on the total entropy generation rate using different values of~~for~~ the interface Biot number. As illustrated, increasing the interface Biot number decreases the total entropy generation rate. This occurs as~~because~~ increasing the interface *Bi*, decreases the temperature difference between the fluid and solid phases, which ultimately decreases the heat transfer between these two phases.~~.~~ That,~~This~~ in turn, decreases the total entropy generation rate. For the parameter values examined in the current study, increasing the Biot number may increase or decrease the total entropy generation rate, as~~which~~ can be clearly seen for *Bi*=5. This is an interesting behaviour, which can lead ~~scholars~~ to the design of superior~~a better~~ systems from the second law perspective.~~,~~ This would be ~~by~~through choosing a suitable porous material and flow condition~~,~~ to ~~finally~~ avoid the maximum entropy generation rate in the channel.

Finally, it is very helpful to examine the main differences between the current results and those of Ref. [39]. In this reference, a similar configuration to that shown in Fig. 1 was analyzed. However, unlike the current investigation, Model A [15,19] was employed to describe the thermal boundary condition of the porous-fluid interface. Some significant disparities between the current results and those of Ref. [39] are clearly visible in the temperature fields. Consideration of Model A in [39] enforced the equality of solid and fluid temperature on the porous-fluid interface. Yet, the convective interface model, used in the current investigation, does not require the equality of the temperatures on this interface. As a result, there could be significant temperature differences between the fluid and solid phases on the interface of the porous insert (see Figs. 2-6). Importantly, modifying the Biot number (Fig. 4) and the exothermicity of the system (Fig. 6) can highly intensify these temperature differences. This implies a stronger deviation from the local thermal equilibrium compared to the predictions of Model A [39]. In addition to the direct influence of the temperature fields upon the Nusselt number (see Eq. (9)), temperature differences within the porous insert, constitutes a major source of irreversibility [38]. It follows that the introduction of a temperature difference on the porous interface by the virtue of utilising the convective interface model can lead to strengthening of entropy generation in the system. This is an essential consequence of altering the porous-fluid thermal interface model, which becomes further significant in systems with exothermicity. Nonetheless, it is important to note that due to the dependency of entropy generation to a large number of parameters and its inherent complexity, this statement should be generalised most cautiously. As discussed earlier, there is, currently, no generally preferred porous-fluid interface model [15,19] and the choice of interface model remains problem dependent [16,17,24]. Previous studies [16,17,23,24] have demonstrated the influences of different interface models on the heat transfer characteristics of partially-filled conduits with a central porous inert. Amongst other findings, the current work and that presented in Ref. [39] extended the earlier findings to the conduits, in which porous inserts are attached to the wall (Fig. 1). Most importantly, for the first time, these works demonstrated the effects of variations in porous-fluid interface models on the entropic behaviour of these systems.

4. Conclusions

Forced convection heat transfer, as well as the local and total generation of entropy in a two-dimensional channel, partially filled with porous materials and subject to constant heat flux, were analyzed theoretically. The two-

equation model of thermal energy transport, on the basis of LTNE, was utilized. A convective model was used as the thermal boundary condition on the porous-fluid interface and Model A [15,19] expressed the solid-porous thermal boundary condition. Semi-analytical expressions were, then, derived for the temperature and velocity fields, the Nusselt number and the total and local entropy generations in the channel. The results showed that the utilization of the convective thermal boundary condition on the porous-fluid interface could significantly modify the behaviour of the temperature fields. It was argued that this has substantial influence on the irreversibility of the system and that the local and total entropy generation within the system are strong functions of the employed porous-fluid interface model. Addition of the internal heat sources, further introduced a variety of trends in the thermal behaviour of the system, as such different routes to the bifurcation of the temperature were observed. It was also shown that the validity of LTE assumption for the problem under investigation is limited to only a very specific set of parameters. Under most conditions, encountered in this study, the temperature difference between the fluid and solid phases was considerable. In keeping with the previous investigations, it was shown that the thickness of the porous inserts in the channel dominates the entropy generation. The level of exothermicity and the thermal conductivity ratio were also observed to have strong effects upon the generation of entropy in the channel. Finally, it was demonstrated that exothermicity in the solid and fluid phases has different effects upon the entropy generation and simultaneous heat generation, in both the solid and fluid can substantially increase the rate of entropy generation.

The findings of this paper clarified the influence of porous-fluid thermal boundary conditions and internal heat generation on the thermal behaviour of partially-filled systems. They further complemented those of the previous work [39] and clearly showed the influence of the variations in the porous-fluid interface model upon the thermal and entropic behaviour of the system under investigation. The results can be also used for the validation of numerical simulations and other theoretical studies.

Acknowledgments

This work was supported by the Hong Kong Research Grants Council (project no. CityU 125412) and NSAF (grant no. U1330132).

Appendix A

A direct comparison of the current work with a similar theoretical or numerical investigation, available in the open literature, is not possible. This is due to the fact that, to the best of our knowledge, the problem under investigation has not been previously tackled. Nonetheless, the LTE solution can be validated against the earlier work of Chen et al. [45]. In conducting such comparison, it should be emphasised that due to differences in the definitions of parameters in the current work and Ref. [45], a large value of k should be selected to approach $\left(\frac{1}{k}+1\right)$ in Eq. ((22b) towards unity. Further, we set $Y_c = 0$ and $\varepsilon = 1$. The relation between the remaining parameters in our study and those in Ref. [45] would be as follows.

$$S^2 = \frac{1}{Da},\ \beta = w_f + w_s \,. \tag{A.1}$$

By choosing any combination of w_f and w_s that results in $\beta = 1$ and varying Da, Fig. 4b of Chen et al. [45] is reproduced. Figure A.1. shows that the temperature files calculated by the current work coincides on that by Ref. [45].

References

[1] Bergman TL, Lavine AS, Incropera FP, DeWitt DP. Introduction to Heat Transfer. 6th ed. John Wiley and Sons, Inc.; 2011.

[2] Bejan A. Entropy Generation Minimization: The Method of Thermodynamic Optimization of Finite-Size Systems and Finite-Time Processes. CRC Press; 1995.

[3] Torabi M, Zhang K. Classical entropy generation analysis in cooled homogenous and functionally graded material slabs with variation of internal heat generation with temperature, and convective–radiative boundary conditions. Energy 2014;65:387–97. doi:10.1016/j.energy.2013.11.020.

[4] Torabi M, Zhang K. Temperature distribution and classical entropy generation analyses in an asymmetric cooling composite hollow cylinder with temperature-dependent thermal conductivity and internal heat generation. Energy 2014;73:484–96. doi:10.1016/j.energy.2014.06.041.

[5] Aziz A, Khan WA. Classical and minimum entropy generation analyses for steady state conduction with temperature dependent thermal conductivity and asymmetric thermal boundary conditions: Regular and functionally graded materials. Energy 2011;36:6195–207. doi:10.1016/j.energy.2011.07.042.

[6] Elazhary AM, Soliman HM. Entropy generation during fully-developed forced convection in parallel-plate micro-channels at high zeta-potentials. Int J Heat Mass Transf 2014;70:152–61. doi:10.1016/j.ijheatmasstransfer.2013.10.060.

[7] Mahian O, Kianifar A, Kleinstreuer C, Al-Nimr MA, Pop I, Sahin AZ, et al. A review of entropy generation in nanofluid flow. Int J Heat Mass Transf 2013;65:514–32. doi:10.1016/j.ijheatmasstransfer.2013.06.010.

[8] Mahian O, Oztop H, Pop I, Mahmud S, Wongwises S. Design of a vertical annulus with MHD flow using entropy generation analysis. Therm Sci 2013;17:1013–22. doi:10.2298/TSCI121017038M.

[9] Vafai K. Porous Media: Applications in Biological Systems and Biotechnology. Boca Raton, FL.: CRC Press; 2011.

[10] Vadasz P, editor. Emerging Topics in Heat and Mass Transfer in Porous Media. Berlin: Springer; 2008.

[11] Nield DA, Bejan A. Convection in Porous Media. 4th editon. New York: Speringer; 2013.

[12] Amiri A., Vafai K. KTM. Effects of boundary conditions on non-Darcian heat transfer through porous

media and experimental comparisons. Numer Heat Transf Part A Appl 1995;27:651–64.

[13] Alazmi B, Vafai K. Constant wall heat flux boundary conditions in porous media under local thermal non-equilibrium conditions. Int J Heat Mass Transf 2002;45:3071–87.

[14] B. Alazmi, Vafai K. Analysis of variants within the porous media transport models. J Heat Transfer 2000;122:303–26.

[15] Yang K, Vafai K. Analysis of heat flux bifurcation inside porous media incorporating inertial and dispersion effects – An exact solution. Int J Heat Mass Transf 2011;54:5286–97. doi:10.1016/j.ijheatmasstransfer.2011.08.014.

[16] Mahmoudi Y, Karimi N. Numerical investigation of heat transfer enhancement in a pipe partially filled with a porous material under local thermal non-equilibrium condition. Int J Heat Mass Transf 2014;68:161–73. doi:10.1016/j.ijheatmasstransfer.2013.09.020.

[17] Mahmoudi Y, Karimi N, Mazaheri K. Analytical investigation of heat transfer enhancement in a channel partially filled with a porous material under local thermal non-equilibrium condition: Effects of different thermal boundary conditions at the porous-fluid interface. Int J Heat Mass Transf 2014;70:875–91. doi:10.1016/j.ijheatmasstransfer.2013.11.048.

[18] Forooghi P, Abkar M, Saffar-Avval M. Steady and unsteady heat transfer in a channel partially filled with porous media under thermal non-equilibrium condition. Transp Porous Media 2011;86:177–98.

[19] Yang K, Vafai K. Restrictions on the validity of the thermal conditions at the porous-fluid interface—An exact solution. J Heat Transfer 2011;133:112601. doi:10.1115/1.4004350.

[20] Xu HJ, Qu ZG, Lu TJ, He YL, Tao WQ. Thermal modeling of forced convection in a parallel-plate channel partially filled with metallic foams. J Heat Transfer 2011;133:092603. doi:10.1115/1.4004209.

[21] Xu HJ, Qu ZG, Tao WQ. Analytical solution of forced convective heat transfer in tubes partially filled with metallic foam using the two-equation model. Int J Heat Mass Transf 2011;54:3846–55. doi:10.1016/j.ijheatmasstransfer.2011.04.044.

[22] Ochoa-Tapia JA, Whitaker S. Momentum transfer at the boundary between a porous medium and a homogeneous fluid—I. Theoretical development. Int J Heat Mass Transf 1995;38:2635–46. doi:10.1016/0017-9310(94)00346-W.

[23] Karimi N, Agbo D, Talat Khan A, Younger PL. On the effects of exothermicity and endothermicity upon the temperature fields in a partially-filled porous channel. Int J Therm Sci 2015;96:128–48. doi:10.1016/j.ijthermalsci.2015.05.002.

[24] Karimi N, Mahmoudi Y, Mazaheri K. Temperature fields in a channel partially filled with a porous material under local thermal non-equilibrium condition - An exact solution. Proc Inst Mech Eng Part C J Mech Eng Sci 2014;288:2778–89. doi:10.1177/0954406214521800.

[25] Hooman K, Ejlali A. Entropy generation for forced convection in a porous saturated circular tube with uniform wall temperature. Int Commun Heat Mass Transf 2007;34:408–19. doi:10.1016/j.icheatmasstransfer.2006.10.008.

[26] Hooman K, Haji-Sheikh A. Analysis of heat transfer and entropy generation for a thermally developing Brinkman-Brinkman forced convection problem in a rectangular duct with isoflux walls. Int J Heat Mass Transf 2007;50:4180–94. doi:10.1016/j.ijheatmasstransfer.2007.02.036.

[27] Hooman K, Gurgenci H, Merrikh AA. Heat transfer and entropy generation optimization of forced convection in porous-saturated ducts of rectangular cross-section. Int J Heat Mass Transf 2007;50:2051–9. doi:10.1016/j.ijheatmasstransfer.2006.11.015.

[28] Hooman K, Ejlali A, Hooman F. Entropy generation analysis of thermally developing forced convection in fluid-saturated porous medium. Appl Math Mech 2008;29:229–37. doi:10.1007/s10483-008-0210-1.

[29] Mahmud S, Fraser RA. Flow, thermal, and entropy generation characteristics inside a porous channel with viscous dissipation. Int J Therm Sci 2005;44:21–32. doi:10.1016/j.ijthermalsci.2004.05.001.

[30] Kamisli F. Analysis of laminar flow and forced convection heat transfer in a porous medium. Transp Porous Media 2009;80:345–71. doi:10.1007/s11242-009-9364-7.

[31] Mahmud S, Tasnim SH, Fraser RA, Pop I. Hydrodynamic and thermal interaction of a periodically oscillating fluid with a porous medium lying over a thick solid plate. Int J Therm Sci 2011;50:1908–19. doi:10.1016/j.ijthermalsci.2011.04.019.

[32] Mahmud S, Fraser RA. Magnetohydrodynamic free convection and entropy generation in a square porous cavity. Int J Heat Mass Transf 2004;47:3245–56. doi:10.1016/j.ijheatmasstransfer.2004.02.005.

[33] Tasnim SH, Shohel M, Mamun MAH. Entropy generation in a porous channel with hydromagnetic effect. Exergy, An Int J 2002;2:300–8. doi:10.1016/S1164-0235(02)00065-1.

[34] Morosuk T V. Entropy generation in conduits filled with porous medium totally and partially. Int J Heat Mass Transf 2005;48:2548–60. doi:10.1016/j.ijheatmasstransfer.2005.01.018.

[35] Shokouhmand H, Jam F, Salimpour MR. Optimal porosity in an air heater conduit filled with a porous matrix. Heat Transf Eng 2009;30:375–82. doi:10.1080/01457630802414664.

[36] Mahdavi M, Saffar-Avval M, Tiari S, Mansoori Z. Entropy generation and heat transfer numerical analysis in pipes partially filled with porous medium. Int J Heat Mass Transf 2014;79:496–506. doi:10.1016/j.ijheatmasstransfer.2014.08.037.

[37] Buonomo B, Manca O, Lauriat G. Forced convection in micro-channels filled with porous media in local thermal non-equilibrium conditions. Int J Therm Sci 2014;77:206–22. doi:10.1016/j.ijthermalsci.2013.11.003.

[38] Torabi M, Zhang K, Yang G, Wang J, Wu P. Heat transfer and entropy generation analyses in a channel partially filled with porous media using local thermal non-equilibrium model. Energy 2015;82:922–38. doi:10.1016/j.energy.2015.01.102.

[39] Torabi M, Karimi N, Zhang K. Heat transfer and second law analyses of forced convection in a channel partially filled by porous media and featuring internal heat sources. Energy 2015;93:106–27. doi:10.1016/j.energy.2015.09.010.

[40] Yang K, Vafai K. Analysis of temperature gradient bifurcation in porous media – An exact solution. Int J Heat Mass Transf 2010;53:4316–25. doi:10.1016/j.ijheatmasstransfer.2010.05.060.

[41] Mahjoob S, Vafai K. Analysis of Bioheat Transport Through a Dual Layer Biological Media. J Heat Transfer 2010;132:031101. doi:10.1115/1.4000060.

[42] Bandhauer TM, Garimella S, Fuller TF. A critical review of thermal issues in lithium-ion batteries. J Electrochem Soc 2011;158:R1–25. doi:10.1149/1.3515880.

[43] Zheng K, Sun Q, Ni M. Local non-equilibrium thermal effects in solid oxide fuel cells with various fuels. Energy Technol 2013;1:35–41. doi:10.1002/ente.201200014.

[44] Ting TW, Hung YM, Guo N. Entropy generation of viscous dissipative nanofluid convection in asymmetrically heated porous microchannels with solid-phase heat generation. Energy Convers Manag 2015;105:731–45. doi:10.1016/j.icheatmasstransfer.2015.09.003.

[45] Chen GM, Tso CP, Hung Yew Mun YM. Field synergy principle analysis on fully developed forced convection in porous medium with uniform heat generation. Int Commun Heat Mass Transf 2011;38:1247–52. doi:10.1016/j.icheatmasstransfer.2011.06.010.

[46] Qu ZG, Xu HJ, Tao WQ. Fully developed forced convective heat transfer in an annulus partially filled with metallic foams: An analytical solution. Int J Heat Mass Transf 2012;55:7508–19. doi:10.1016/j.ijheatmasstransfer.2012.07.048.

[47] Yang C, Nakayama A, Liu W. Heat transfer performance assessment for forced convection in a tube partially filled with a porous medium. Int J Therm Sci 2012;54:98–108. doi:10.1016/j.ijthermalsci.2011.10.023.

[48] Mahian O, Mahmud S, Heris SZ. Analysis of entropy generation between co-rotating cylinders using nanofluids. Energy 2012;44:438–46. doi:10.1016/j.energy.2012.06.009.

[49] Yazdi MH, Abdullah S, Hashim I, Sopian K. Entropy generation analysis of open parallel microchannels embedded within a permeable continuous moving surface: application to magnetohydrodynamics (MHD). Entropy 2011;14:1–23. doi:10.3390/e14010001.

[50] Torabi M, Zhang K. Temperature distribution, local and total entropy generation analyses in MHD porous channels with thick walls. Energy 2015;87:540–54. doi:10.1016/j.energy.2015.05.009.

[51] Aziz A, Torabi M. Transient response and entropy generation minimisation of a finite size radiation heat shield with finite heat capacity and temperature-dependent emissivities. Int J Exergy 2013;12:87. doi:10.1504/IJEX.2013.052545.

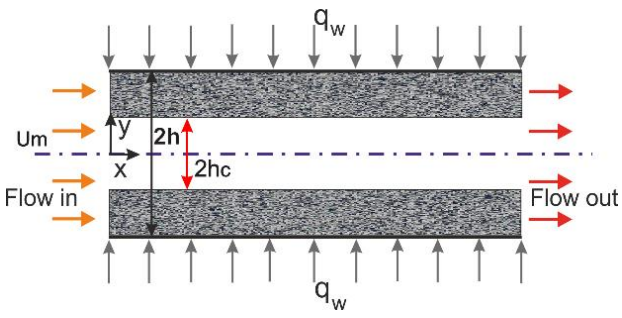

Fig. 1. Configuration of the channel partially filled with a porous material.

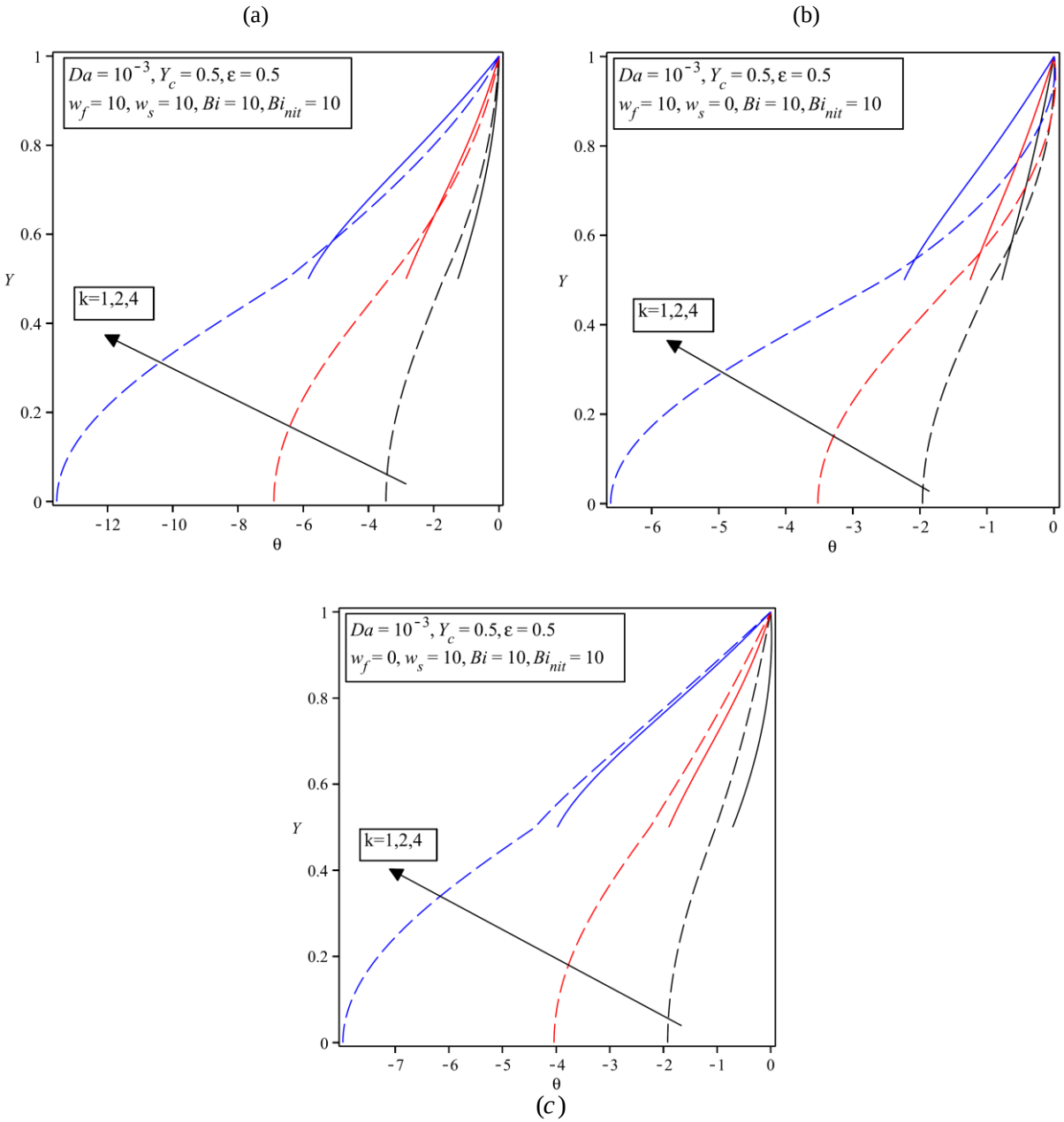

Fig. 2. Dimensionless temperature distribution for different values for the thermal conductivity ratio, $Da = 10^{-3}$

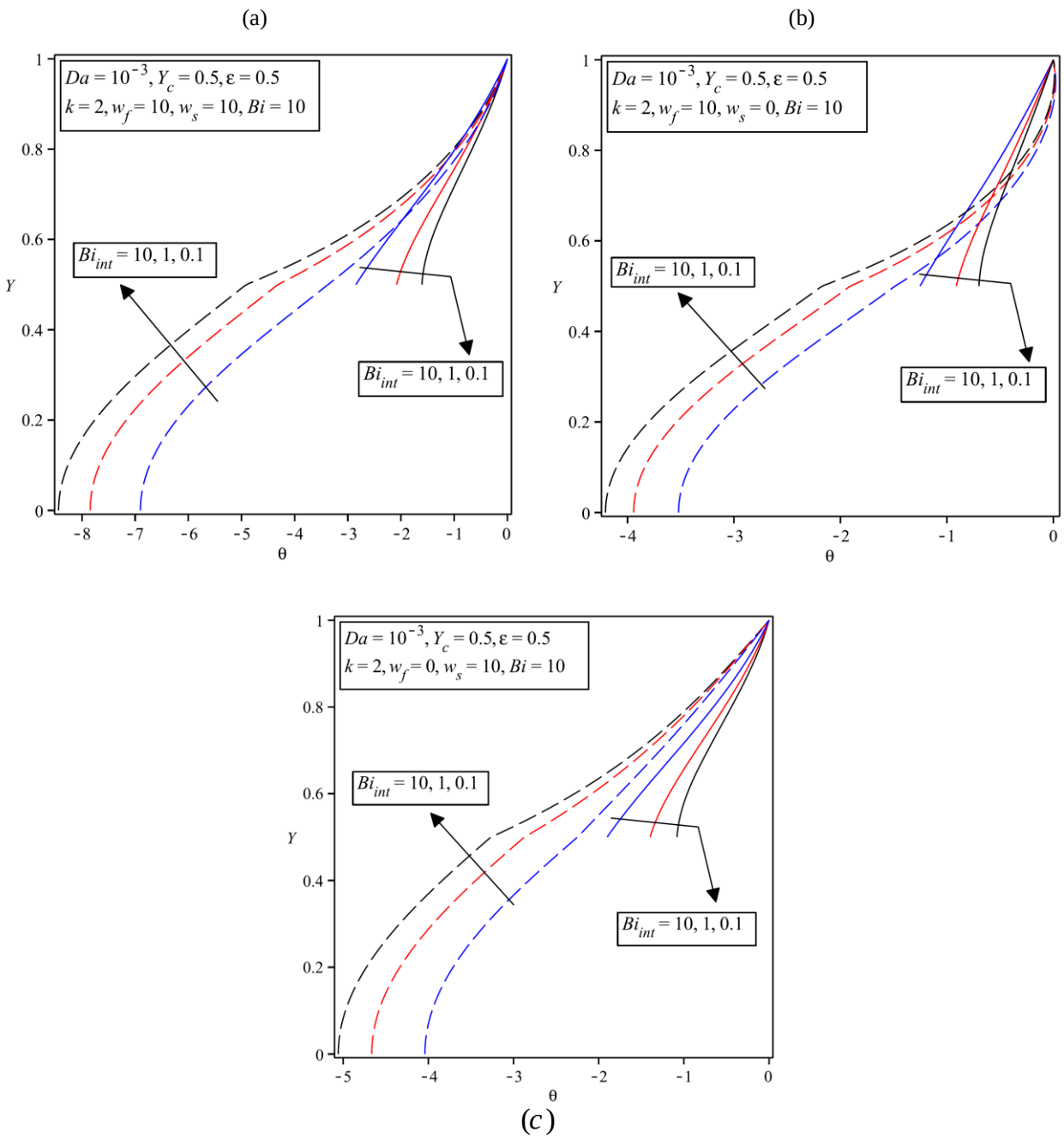

Fig. 3. Dimensionless temperature distribution for different values of interface Biot numbers

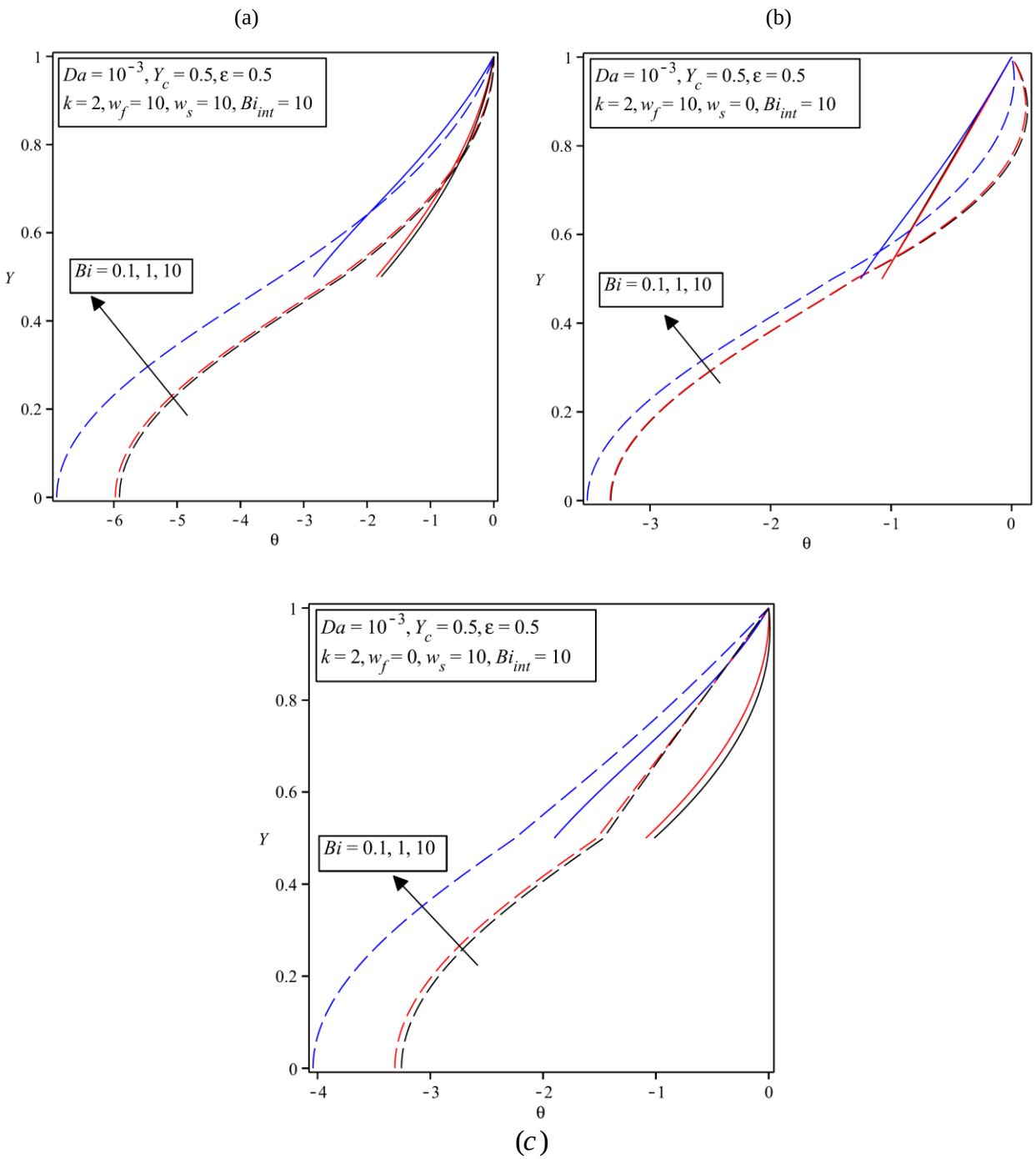

Fig. 4. Dimensionless temperature distribution for different values of Biot numbers

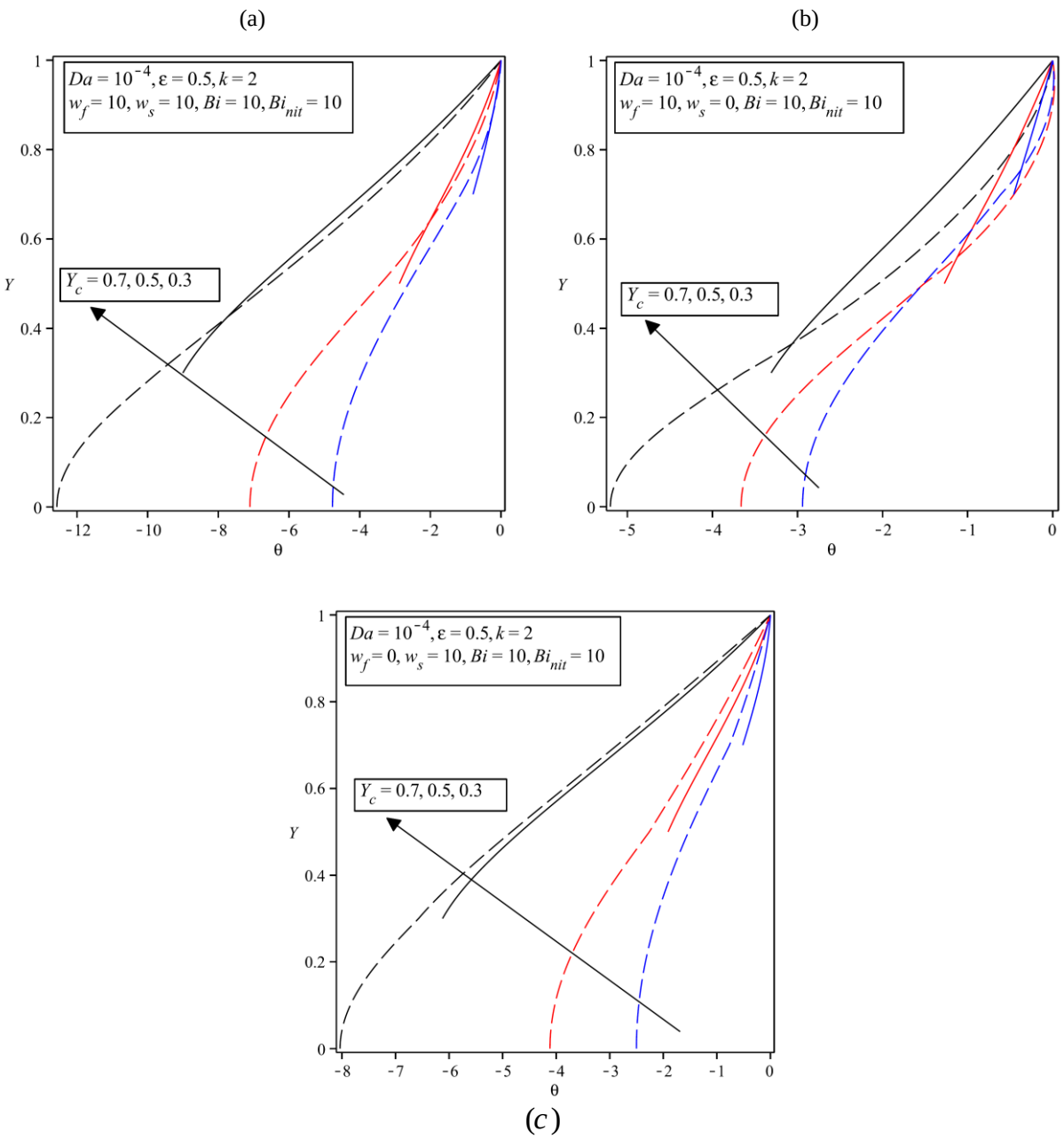

Fig. 5. Dimensionless temperature distribution for different values of the clear section thickness.

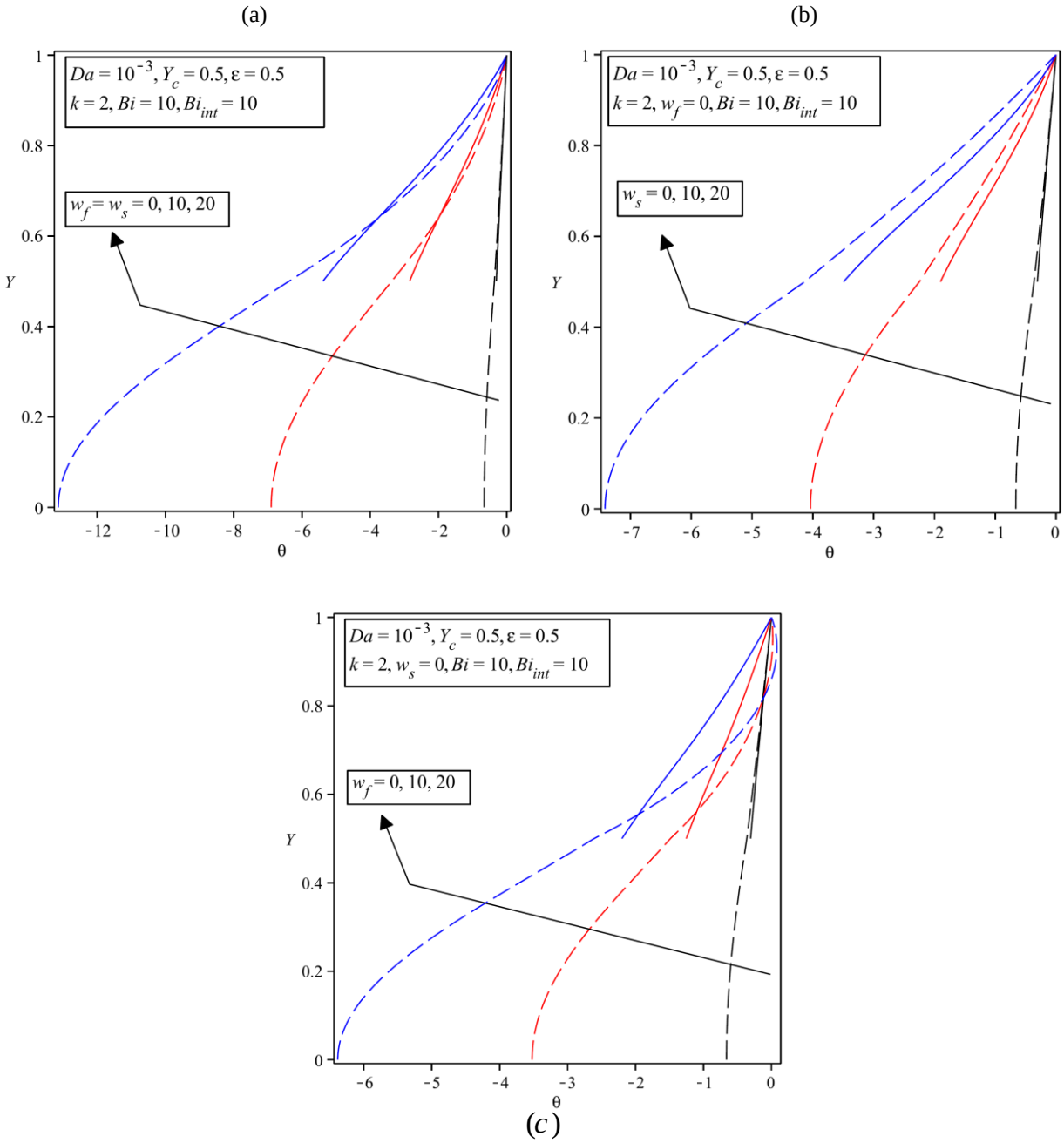

Fig. 6. Dimensionless temperature distribution for different values of the energy source terms

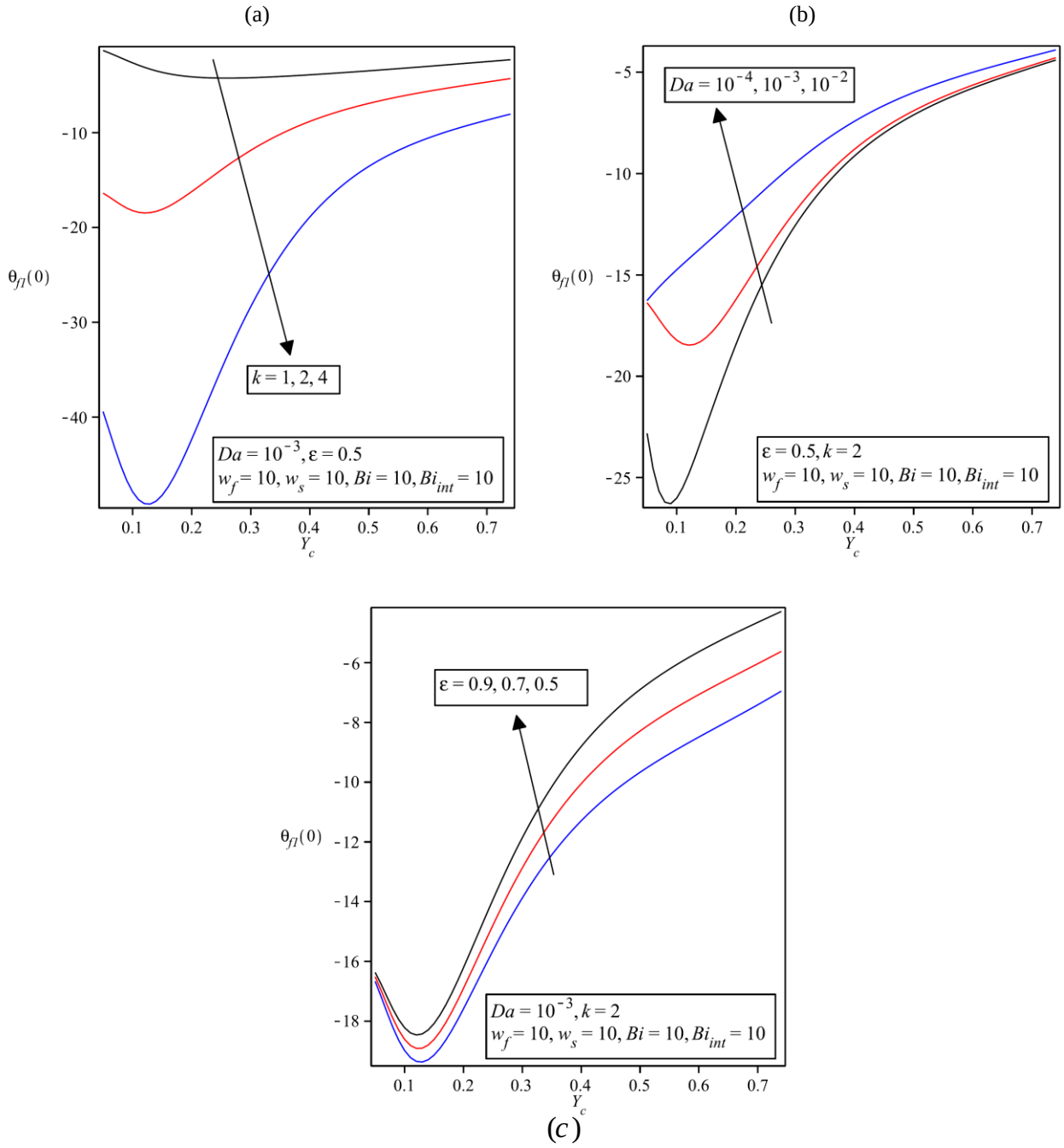

Fig. 7. Dimensionless temperature on the centreline of the channel versus the clear section thickness for varying, (a) thermal conductivity ratio, (b) Darcy number (c) porosity.

.

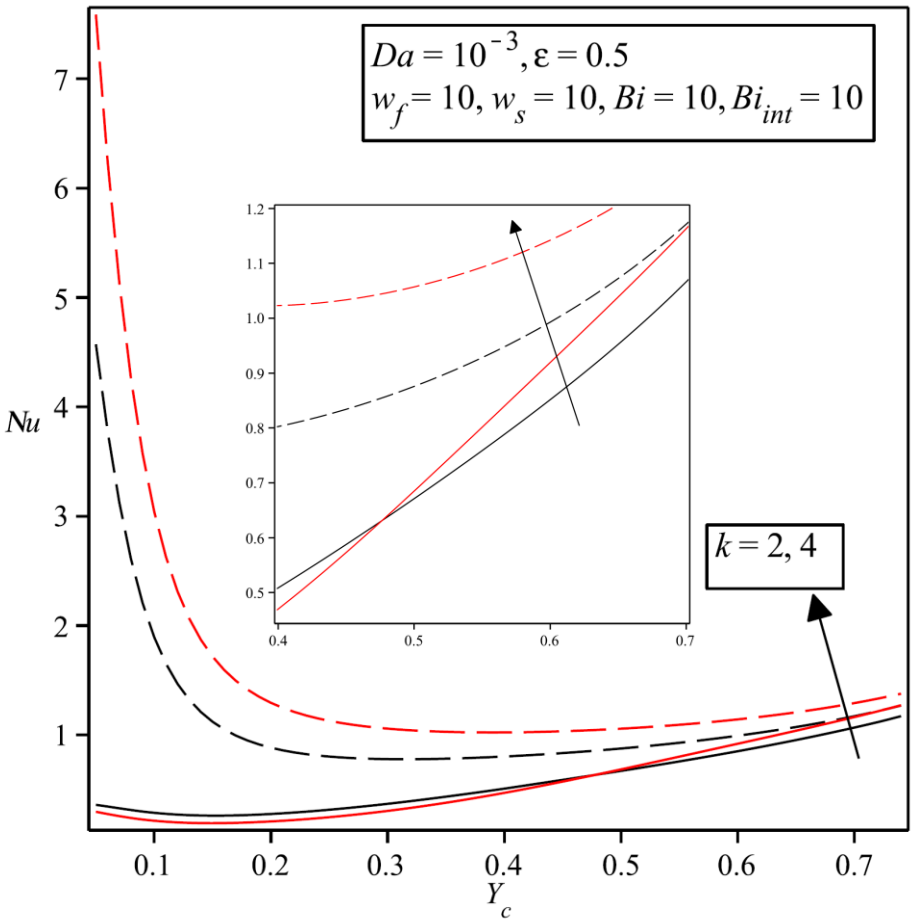

Fig. 8. Nusselt number versus the clear section thickness for both LTNE (solid line) and LTE (dash line) models.

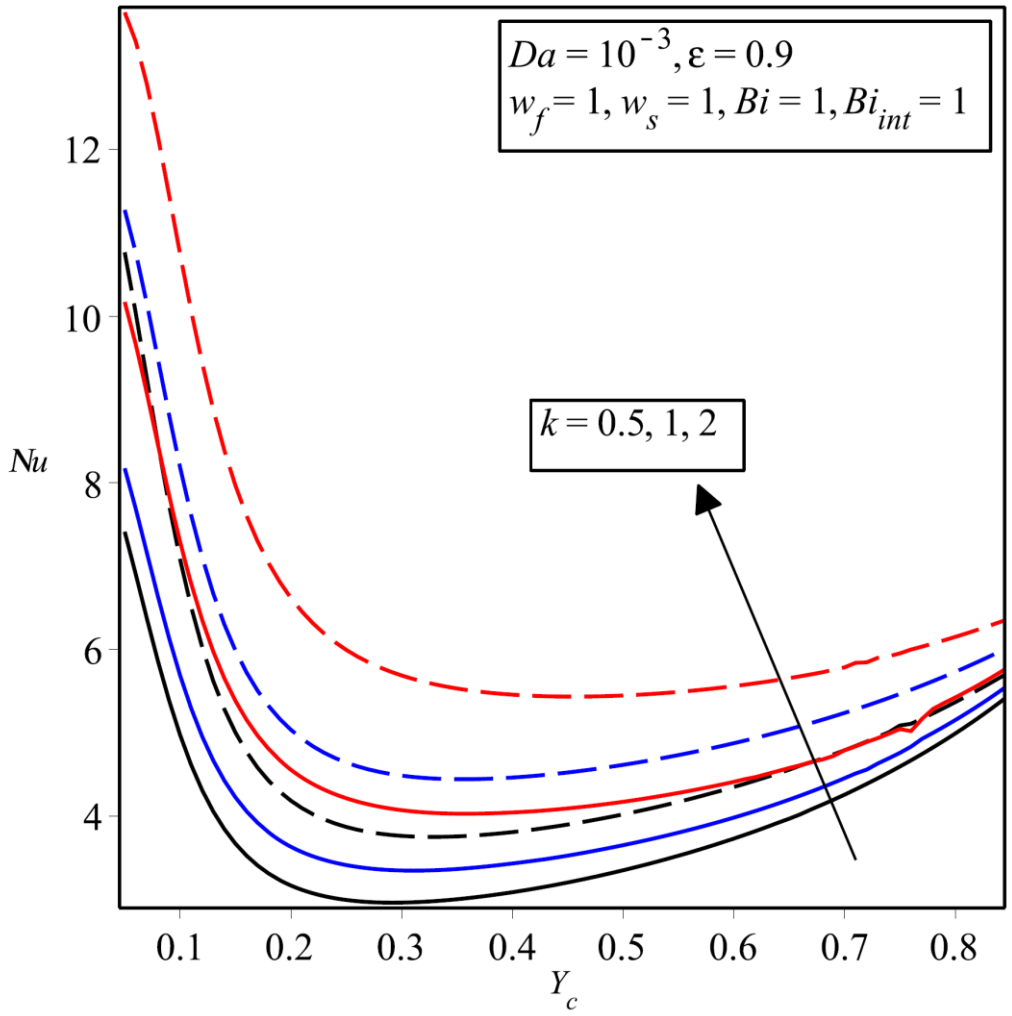

Fig. 9. Nusselt number versus the clear section thickness for different values of thermal conductivity ratios; A comparison between the present analysis (solid lines) and provided calculations in Ref. [39] (dash lines).

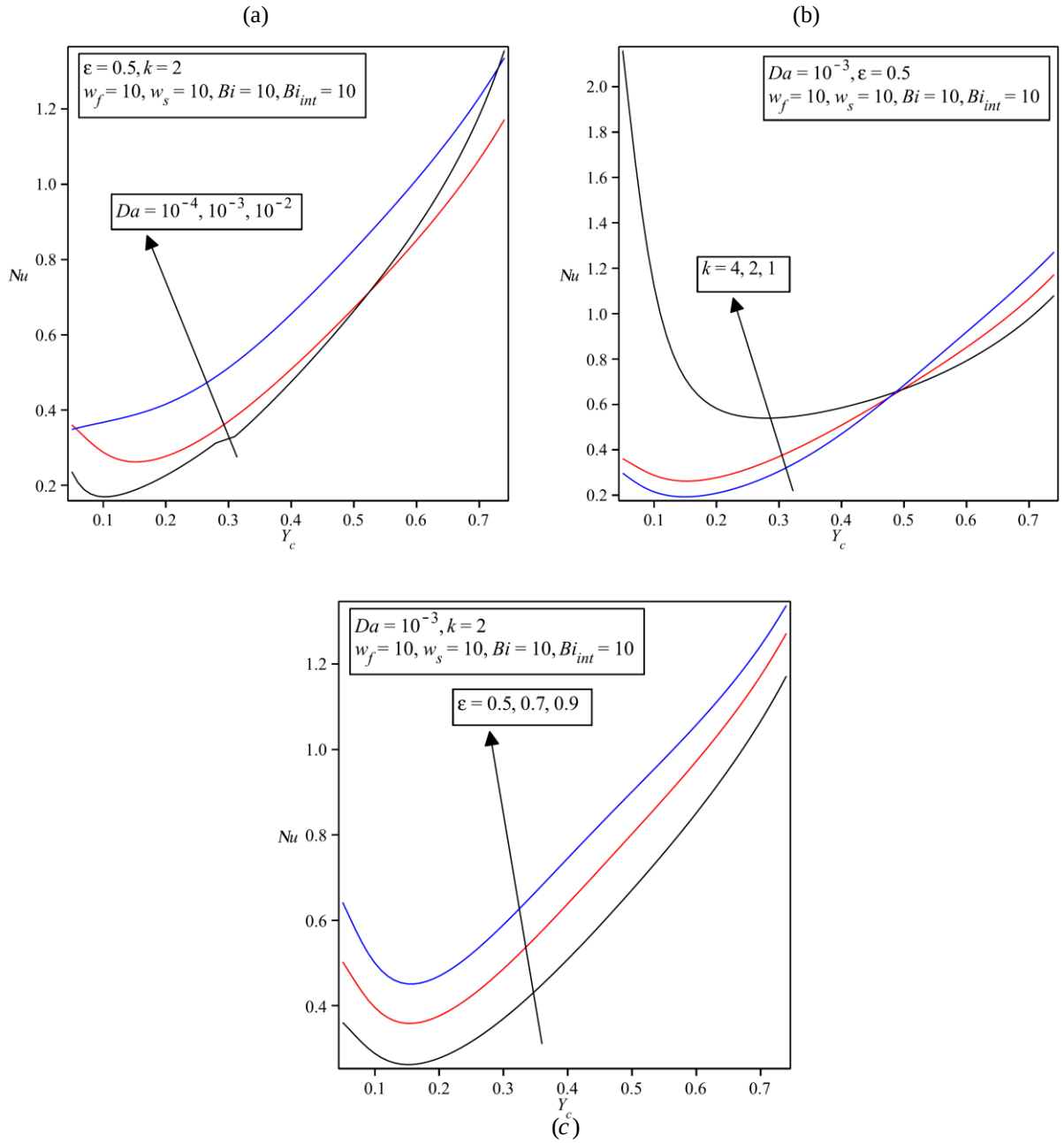

Fig. 10. Nusselt number versus the clear section thickness for different (a) Darcy, (b) thermal conductivity ratio, (c) porosities.

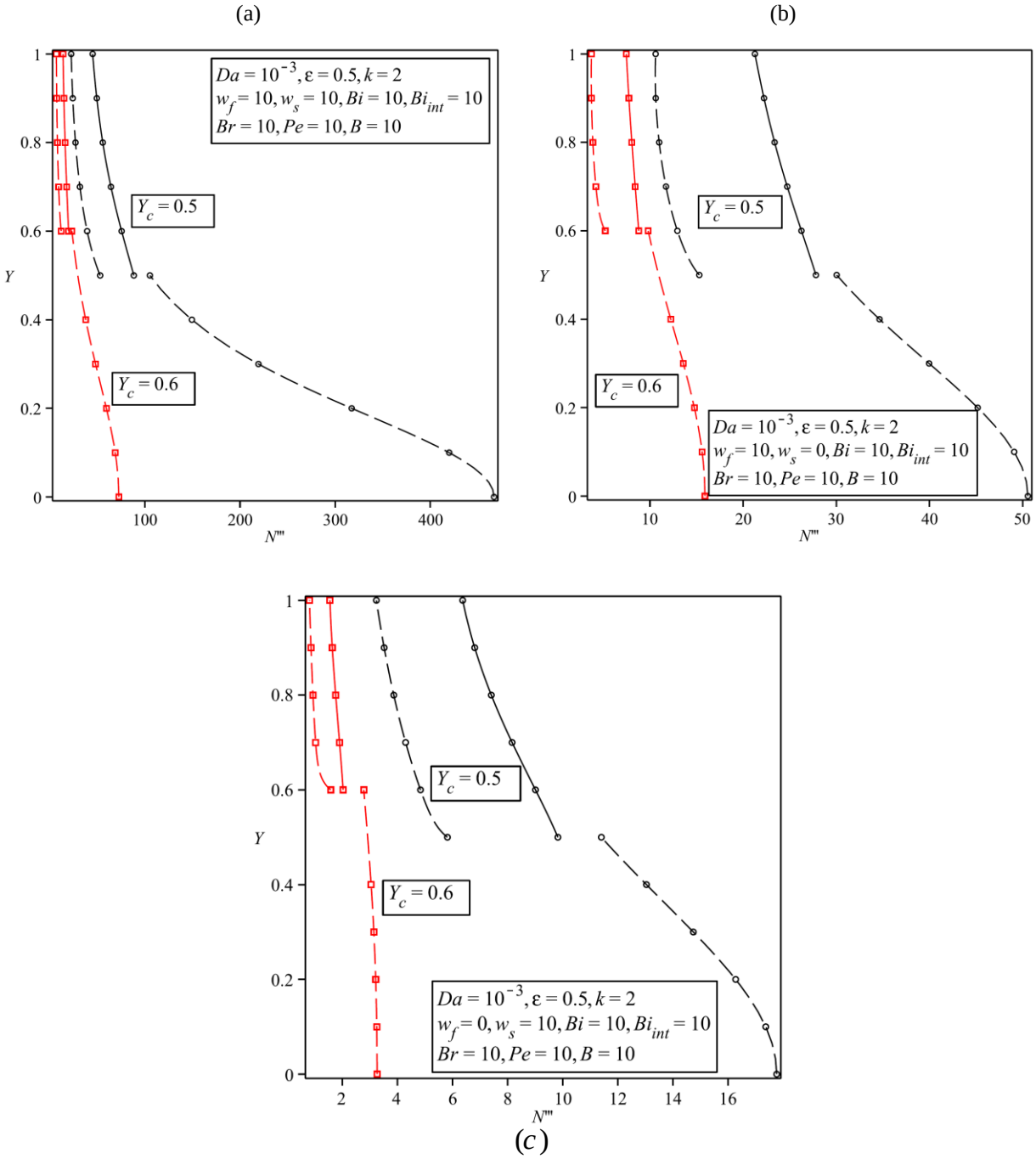

Fig. 11. Local entropy generation rate for $Y_c = 0.5$ and $Y_c = 0.6$.

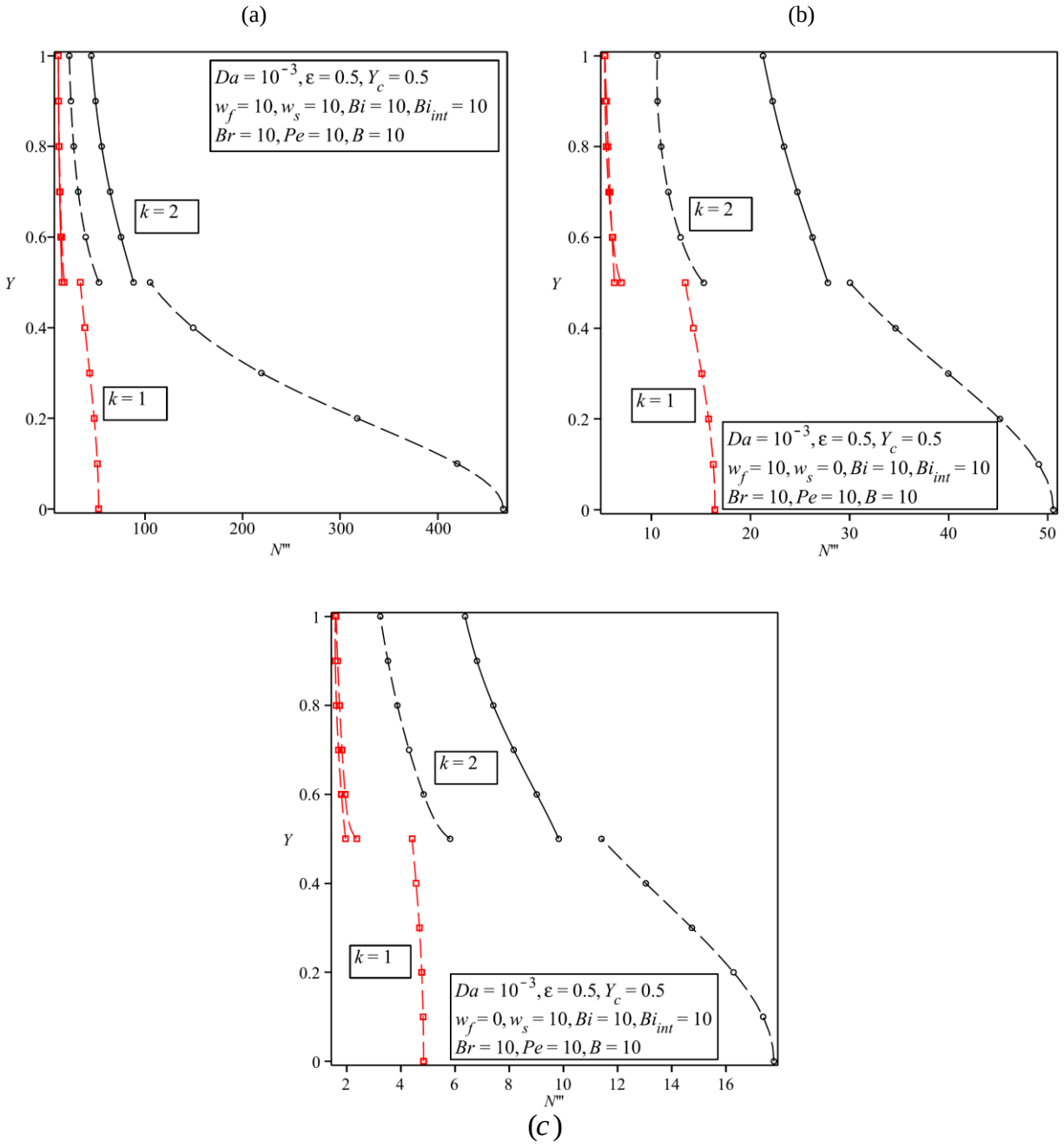

Fig. 12. Local entropy generation rate for two different thermal conductivity ratios.

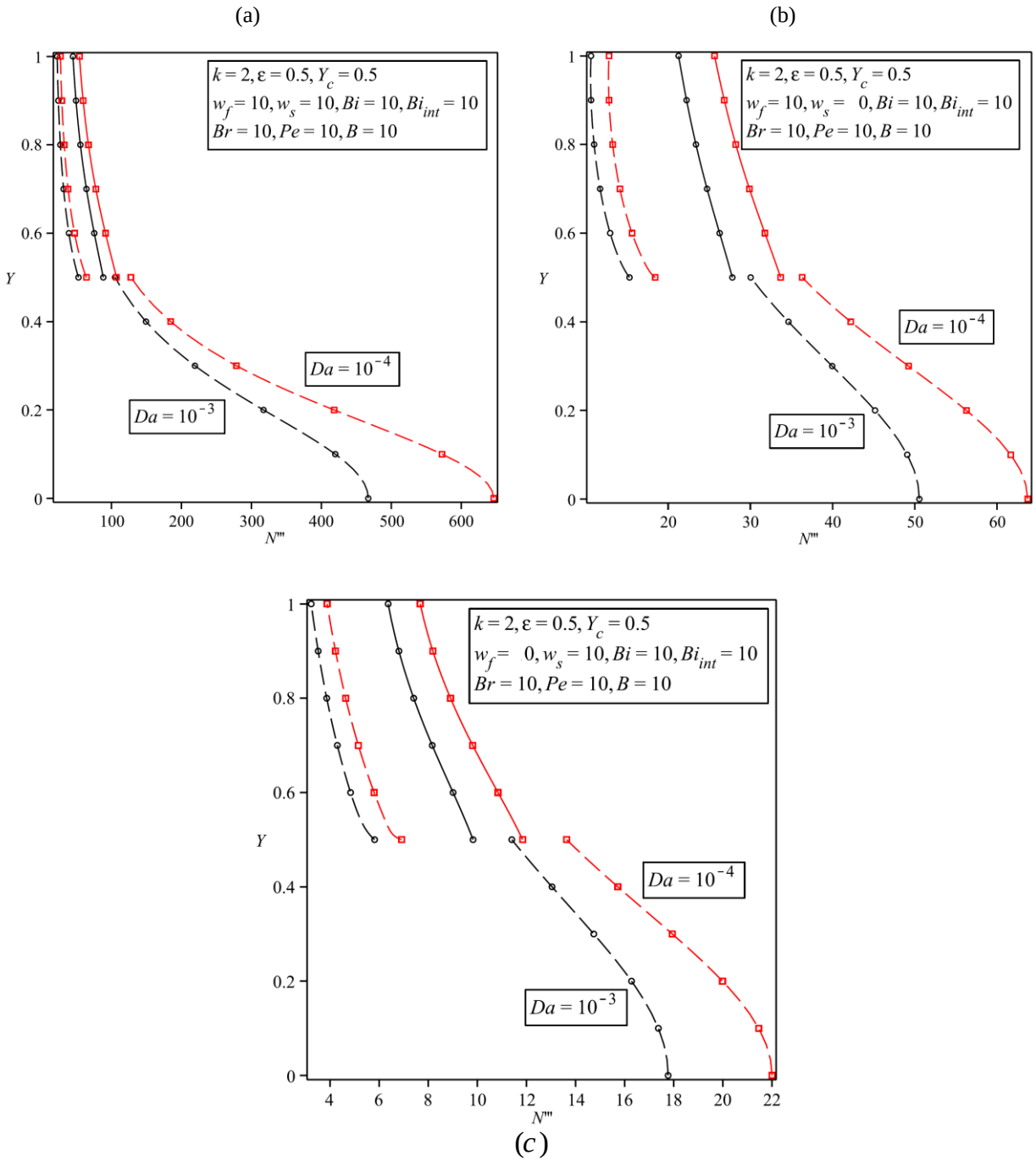

Fig. 13. Local entropy generation rate for two different Darcy numbers.

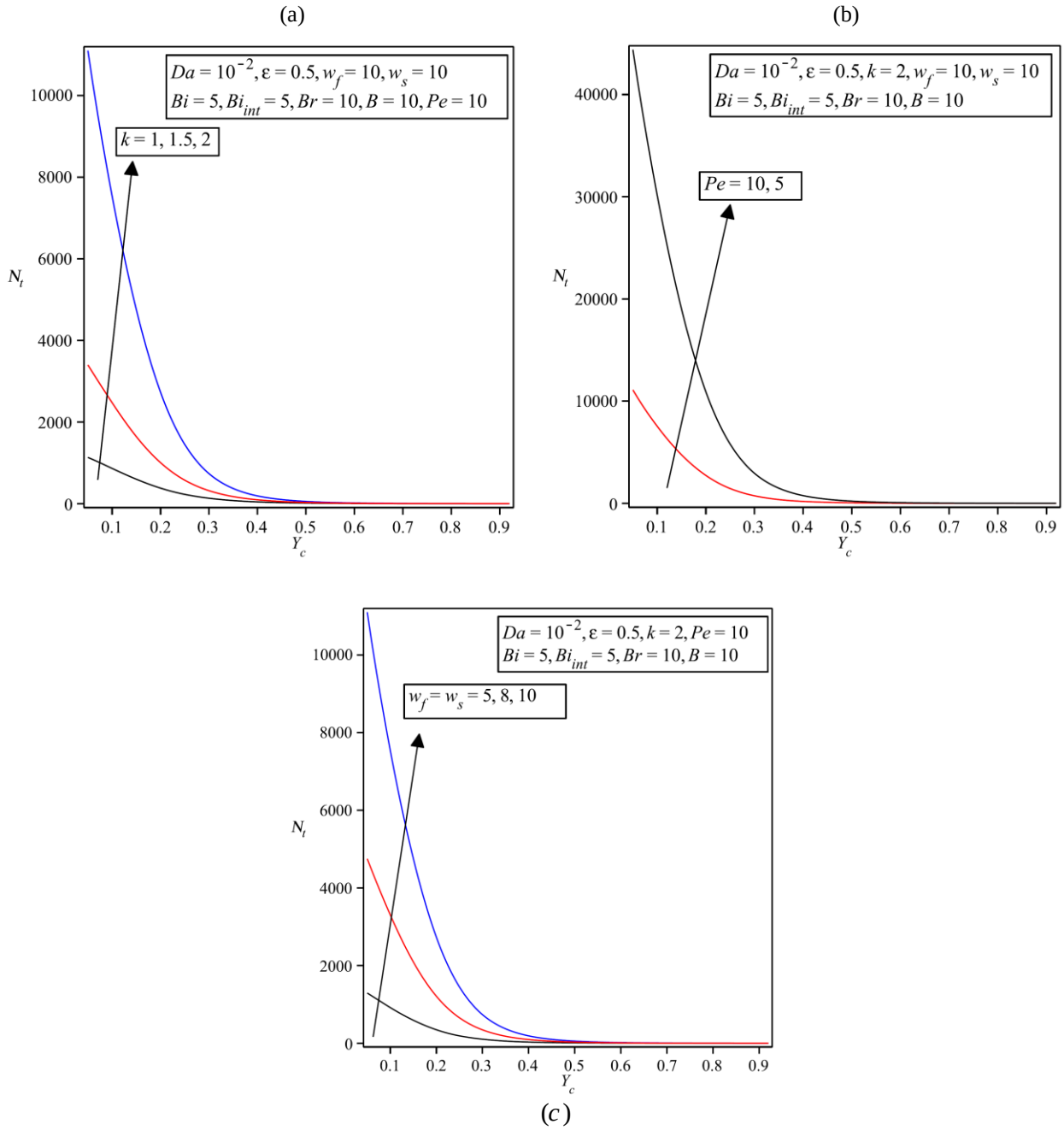

Fig. 14. Total entropy generation rate versus the clear section thickness for different (a) thermal conductivity ratio, (b) Peclet number, (c) energy sources.

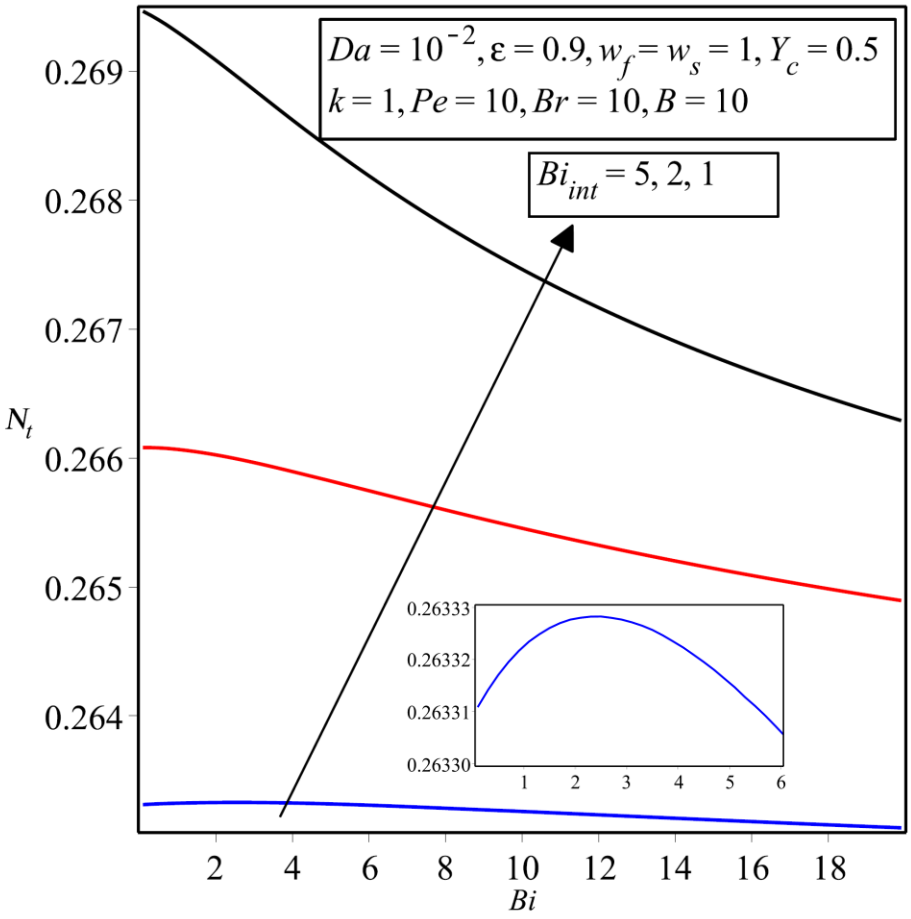

Fig. 15. Total entropy generation rate versus Biot number with different values for interface Biot number.

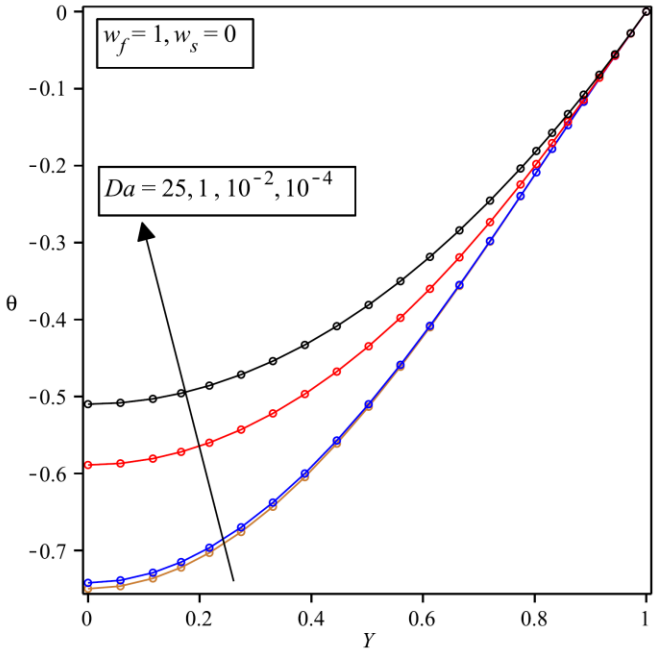

Fig. A.1. Comparison between temperature distribution using LTE model in the present study (solid line) and Chen et al. [45] (circle).